Journal of Medicinal Chemistry

ARTICLE

pubs.acs.org/jmc

Oxime Amides as a Novel Zinc Binding Group in Histone Deacetylase Inhibitors: Synthesis, Biological Activity, and Computational Evaluation

Cinzia B. Botta,[‡] Walter Cabri,[*,⊥] Elena Cini,[†] Lucia De Cesare,[∥] Caterina Fattorusso,[*,∥] Giuseppe Giannini,[⊥] Marco Persico,[∥] Antonello Petrella,[‡] Francesca Rondinelli,[∥] Manuela Rodriquez,[*,‡,§] Adele Russo,[†] and Maurizio Taddei[†]

[†]Dipartimento Farmaco Chimico Tecnologico, Università degli Studi di Siena, Via A. Moro 2, I-53100 Siena, Italy

[‡]Dipartimento di Scienze Farmaceutiche e Biomediche, Università di Salerno, Via Ponte don Melillo, I-84084 Fisciano (SA), Italy

[§]Department of Chemistry and Chemical Biology, Harvard University, 12 Oxford Street, Cambridge, Massachusetts 02138, United States

[∥]Dipartimento di Chimica delle Sostanze Naturali, Università di Napoli, Via D. Montesano, 49 I-80131 Napoli, Italy

[⊥]Chemistry and Analytical Development, R&D Sigma-Tau S.p.A., Via Pontina, km 30,400 I-00040 Pomezia (RM), Italy

Supporting Information

ABSTRACT: Several oxime containing molecules, characterized by a SAHA-like structure, were explored to select a potentially new biasing binding element for the zinc in HDAC catalytic site. All compounds were evaluated for their in vitro inhibitory activity against the 11 human HDACs isoforms. After identification of a "hit" molecule, a programmed variation at the cap group and at the linker was carried out in order to increase HDAC inhibition and/or paralogue selectivity. Some of the new derivatives showed increased activity against a number of HDAC isoforms, even if their overall activity range is still far from the inhibition values reported for SAHA. Moreover, different from what was reported for their hydroxamic acid analogues the new α-oxime amide derivatives do not select between class I and class II HDACs; rather they target specific isoforms in each class. These somehow contradictory results were finally rationalized by a computational assisted SAR, which gave us the chance to understand how the oxime derivatives interact with the catalytic site and justify the observed activity profile.

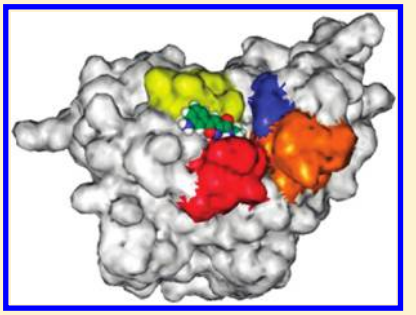

INTRODUCTION

Histone deacetylases (HDACs) are enzymes involved in the remodeling of chromatin and have a key role in the epigenetic regulation of gene expression, as they remove the acetyl moiety from the ε-amino group of lysine side chains of histone and non-histone proteins. High levels of histone acetylation are associated with increased transcriptional activity, whereas low levels of acetylation are associated with repression of gene expression. Eighteen HDACs, subdivided into four classes, have been identified in humans. Class I (HDACs 1, 2, 3, and 8), class IIa (HDACs 4, 5, 7, and 9), class IIb (HDACs 6 and 10), and class IV (HDAC 11) operate as Zn dependent enzymes, have distinct gene expression patterns, and have different cellular location and function. Inhibition of HDACs causes histone hyperacetylation with contemporary transcriptional activation of genes associated with cell cycle arrest or apoptosis in tumor cells. Indeed, several types of HDAC inhibitors have been found to have potential anticancer activity with remarkable tumor specificity.[1] A number of HDAC inhibitors (HDACIs) reached clinical trials, and two of them were lately approved by FDA: suberoylanilide hydroxamic acid (SAHA) from Merck and depsipeptide (FK228) from Gloucester Pharmaceuticals, both for use in cutaneous T-cell lymphoma (CTCL).[2] Moreover, the prospects of using HDACIs as therapeutic interventions for diseases other than cancer are evidenced by the growing number of papers detailing the use of HDACIs in immunomodulation, neurodegeneration, protozoan infections, inflammatory, and heart diseases.[3]

The largely accepted pharmacophore model for most of the known hydroxamic acid derivatives inhibitors consists of (a) a capping group that interacts with the residues at the active site entrance (cap), (b) a zinc binding group (ZBG) that coordinates to the catalytic metal atom within the active site, and (c) a linker that binds to the hydrophobic channel and helps Cap and ZBG to find the correct position. Although SAHA contains a hydroxamic acid moiety and is considered a pan-inhibitor, some data suggest that selectivity toward a specific HDAC might be useful to find more effective inhibitors with limiting side effects. Modifications

Received: October 21, 2010
Published: March 18, 2011

Chart 1. SAHA (1) and Oxime Derivatives 2−5

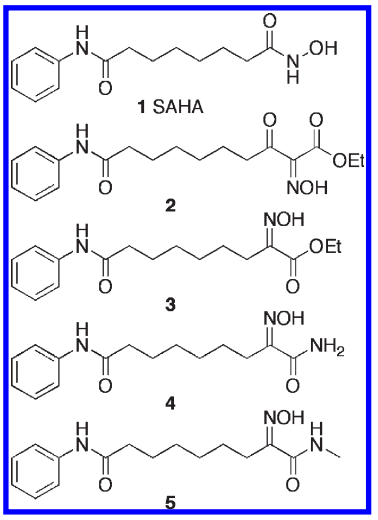

of the Cap, linker, or ZBG have been demonstrated to increase selectivity.[4] Moreover, hydroxamic acid, a strong zinc chelator, presents metabolic and pharmacokinetic issues such as glucuronidation, sulfation, and enzymatic hydrolysis that result in a short in vivo half-life.[5]

Consequently, there are many ongoing research activities to find replacement groups of hydroxamic acid with the dual target of reducing side effects and increasing paralogue selectivity. Many different moieties have been proposed as hydroxamic acid surrogates yielding encouraging results.[6]

Following our interest in this field,[7] we focused on the replacement of the hydroxamic group to find some potent non-hydroxamate small-molecule HDAC inhibitors and to investigate on the paralogue selectivity in order to identify key elements for selective HDAC inhibition. In addition, in terms of chemical biology research, the discovery of novel ZBGs may lead to new types of HDAC isozyme selective inhibitors that are useful tools for probing the biology of the enzyme.[8]

Oxime-containing molecules caught our attention, as they appear to be amenable to biotransformation and conjugations with organic and inorganic molecules. The properties of these classes of compounds have been recently exploited with the aim to design and develop novel therapeutic agents that can display acyl group transfer capabilities and serve for the evaluation of novel candidate drugs for the treatment of various diseases. For example, furan oximes were found to inhibit DNA, RNA, and protein synthesis in lipoid leukemia cells.[9] Derivatives of quinoline oximes were also shown to possess antitumor activity,[10] and glucosinolates were suggested as cancer preventive agents. The stability of oxime complexes with various metals has been shown to result in promising compounds with antitumor activity, such as cis and trans platinum complexes[11] and homo- and heteronuclear Cu(II) and Mn(II) oxime complexes.[12] A complex of technetium with hexamethylpropyleneamine oxime was also used to monitor photodynamic therapy of prostate tumors.[13]

On the basis of these considerations, several oxime containing molecules characterized by a SAHA-like structure were explored selecting those where a mimetic of the natural substrates chelating features were possible, such as α-oxime esters and α-oxime amides (compounds **2**−**5** in Chart 1). After identification of **5** as a "hit" molecule, a programmed variation at the cap group and at the linker was carried out in order to increase the activity and/or paralogue selectivity. The results were finally rationalized by a computational assisted SAR, which gave us the chance to understand how the oxime derivatives interact with the catalytic site and justify the observed activity profile.

Scheme 1. Synthesis of Keto Oxime Ester 2[a]

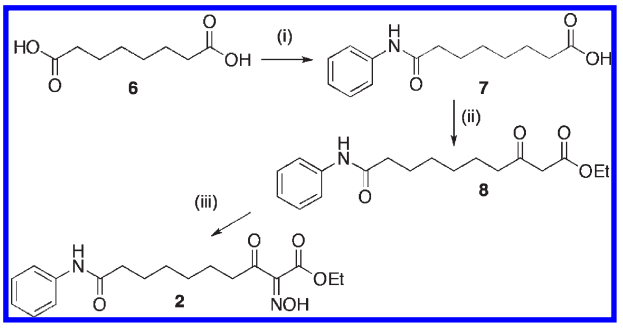

[a] Reagents and conditions: (i) (1) Ac_2O, 140 °C, 39%; (2) aniline, THF, room temp, 74%; (ii) CDI, room temp, THF, $CH_2(CO_2Et)_2$, $Mg(OEt)_2$, room temp, THF, 91%; (iii) $NaNO_2$, AcOH, room temp, 80%.

CHEMISTRY

Oxime derivatives employed in this study were prepared following the different routes described in Schemes 1−4. Suberic acid (**6**) was acetylated with Ac_2O and further reacted with aniline to generate monoamide **7** (Scheme 1). Activation of the carboxylic group with CDI followed by reaction with the magnesium salt of diethyl malonate gave keto ester **8** which was eventually oxidized with $NaNO_2$ in acetic acid to form keto oxime ester **2** in good overall yields.

For the synthesis of other oximes correlated to structures **3**−**5**, commercially available ethyl 7-bromo-heptanoate **9** underwent hydrolysis, benzylation, and direct halogen exchange, yielding benzyliodo derivative **10** (Scheme 2). Reaction with diethyl malonate and NaH afforded compound **11** in 88% yield. The benzyl protection was removed by hydrogenolysis (Pd/C, H_2, 1 atm) to give acid **12**. This compound was the key intermediate for the synthesis of **3**−**5** and **14**−**24**, as it enables the introduction of different arylamides at the carboxylic position in order to optimize the Cap. After transformation of **12** into the corresponding acyl chloride, reaction with aniline generated compound **13** in overall 80% yield. The amide was then transformed into the corresponding α-oxime ester **3** with ethyl nitrite and sodium ethoxide. This transformation passes through the formation of the nitroso derivative, which is further cleaved by sodium ethoxide to give the sodium salt of the oxime ester and diethyl carbonate.[14] This reaction gave exclusively one isomer (NMR and HPLC analysis). X-ray analysis of the crystals obtained from compound **3** showed that the oxime was in the *E* configuration (Figure 1SI in Supporting Information). Since all the other oximes were obtained as single diastereomers, the configuration of the oxime moiety of all the other compounds was consequently assigned. The ethyl ester **3** was then transformed into the corresponding amide **4** or methylamide **5** in good yields by reaction with aqueous ammonia or methylamine in ethanol respectively. Amides **14**−**19** were then prepared by coupling of **12** with the corresponding arylamines followed by transformation of the malonic ester into the oxime ester and final amidation.

dx.doi.org/10.1021/jm101373a |*J. Med. Chem.* 2011, 54, 2165–2182

Scheme 2. Synthesis of Oximes 3−5 and 14−24[a]

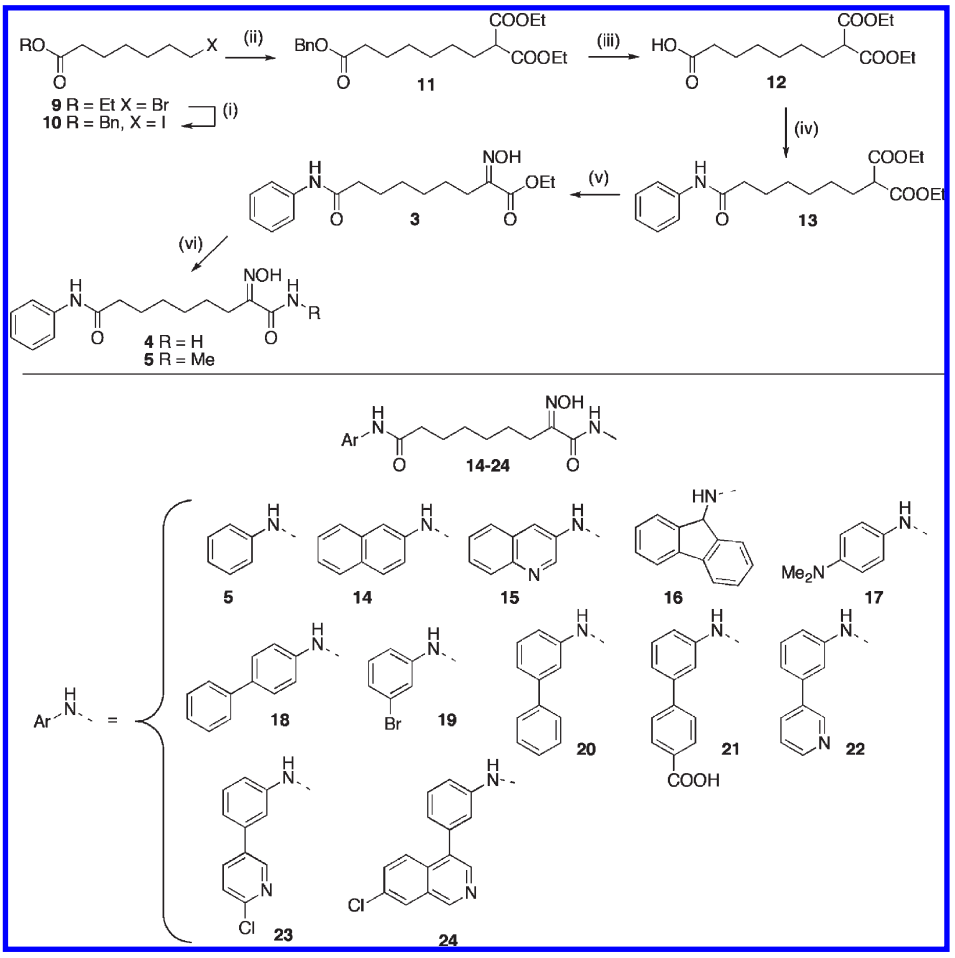

[a] Reagents and conditions: (i) (1) LiOH, EtOH/THF/H_2O 1:1:1, room temp; (2) BnOH, EDC, DMAP, 0 °C to room temp; (3) NaI, acetone, room temp, overall 87%; (ii) $NaCH(CO_2Et)_2$, THF, 0 °C to room temp, 88%; (iii) H_2 (1 atm), Pd/C, $CHCl_3$, 96%; (iv) (1) $(COCl)_2$, DMF, CH_2Cl_2, room temp, 2 h; (2) aniline, Et_3N, CH_2Cl_2, 0 °C to room temp, overall 80%; (v) $C_2H_5NO_2$, NaOEt, EtOH, −5 °C, 92%. (vi) **4**: NH_4OH conc, room temp, 90%. **5**: $MeNH_2$ (33 wt % in ethanol), room temp, 80%.

Amide **19** was used to introduce a substituent in the meta position through a Suzuki coupling in order to increase the size of the cap group and to get more data useful for a comprehensive SAR study. It was possible to carry out the coupling on the free oxime amide with a selected catalyst and conditions as reported in Table 1SI in Supporting Information.

It is interesting to note that the use of microwave dielectric heating (in combination with $Pd(PPh_3)_2Cl_2$) provides exclusively compounds **20**−**22**, while for the preparation of amides **23**−**24** conventional long time heating is required.

Oxime amides **30**−**33** were prepared by coupling of amino derivative **29** with arylisoxazolecarboxylic acids[15] as reported in Scheme 3. Commercially available 6-aminohexanol **25** was first transformed into the aldehyde **26** and immediately submitted to Knoevenagel reaction with diethyl malonate with piperidine/DMF followed by hydrogenation of the double bond giving **27** in 53% overall yield. The malonic ester was treated with ethyl nitrite and sodium ethoxide, affording the α-oxime ester **28**. After transformation of the ethyl ester into the corresponding methylamide, the Boc protecting group was removed with TFA to give the amine **29** in good yields. In order to carry out the reaction between the previously described 5-(3-*tert*-butoxycarbonylaminophenyl)isoxazole-3-carboxylic acid and 5-(4-*tert*butoxycarbonylaminophenyl)isoxazole-3-carboxylic acid with the amine **29**, carrying unprotected oxime group, several coupling agents were then explored.[15]

The most selective reaction occurred using DMTMM[16] in the presence of 1-methylmorpholine, with the formation of compounds **30** and **31** in good yields. Final removal of the Boc with TFA gave the aniline derivatives **32** and **33** in good yields.

The introduction of a stereocenter (with *S* configuration) close to the carboxyamido group was often required in order to obtain a more potent inhibitor.[17] This goal was accomplished starting from (*S*)-glutamic acid (Scheme 4) protected as the tetrabenzyl derivative and further transformed into aldehyde **34** as described in the literature.[18]

Treatment with vinylmagnesium bromide gave the allylic alcohol with contemporary formation of lactone **35** as a mixture of diastereoisomers. The lactone was opened with aniline in the presence of $AlMe_3$ and the hydroxyl group acetylated. The allyl acetate **36** was submitted to a Tsuji−Trost reaction with sodium malonate in the presence of $Pd(PPh_3)_2Cl_2$ that gave compounds **37a** and **37b** in a 2:1 ratio. Complete hydrogenation/hydrogenolysis of the mixture followed by reductive amination with *p*-methoxybenzaldehyde in the presence of $NaBH(OAc)_3$ yielded compound **38**, which was separated from the corresponding regioisomer originating from **37b** and isolated in 46% overall yield.

dx.doi.org/10.1021/jm101373a |*J. Med. Chem.* 2011, 54, 2165–2182

Scheme 3. Synthesis of Oxime Amides 30−33[a]

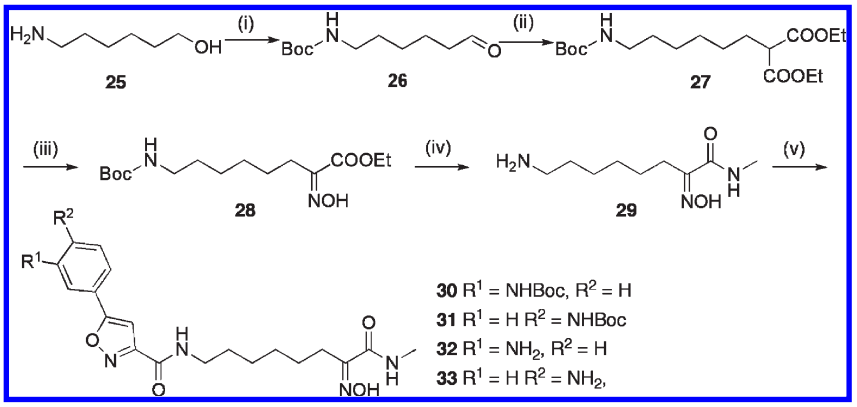

[a] Reagents and conditions: (i) 1) Boc_2O, Et_3N, DCM, room temp, 12 h, 88%; (2) $(COCl)_2$, DMSO, Et_3N, CH_2Cl_2, −78 °C, 30 min, 82%; (ii) (1) $CH_2(COOEt)_2$ DMF, piperidine, room temp, 1 h, 65%; (2) H_2 (1 atm), PtO_2, MeOH, room temp, 1 h, 92%; (iii) $C_2H_5NO_2$, NaOEt, EtOH, −15 °C, 5 h, 61%; (iv) (1) NH_2Me, EtOH, room temp, 12 h, 75%; (2) TFA, DCM, room temp, 12 h, 67%; (v) 5-(3-*tert*-butoxycarbonylaminophenyl)isoxazole-3-carboxylic acid and 5-(4-*tert*-butoxycarbonylaminophenyl)isoxazole-3-carboxylic acid, respectively, DMTMM, NMM, THF, room temp, 12 h.

Scheme 4. Synthesis of Chiral Oxime Amides 40, 41, and 43[a]

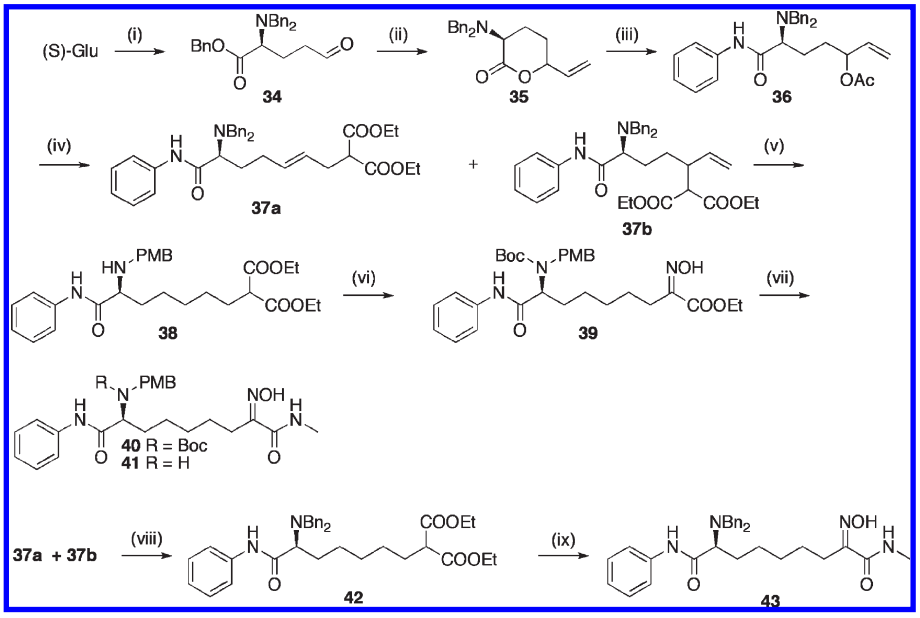

[a] Reagents and conditions: (i) see ref 18; (ii) $CH_2CHMgBr$, THF, 0 °C to room temp, 60%; (iii) (1) aniline, $AlMe_3$, CH_2Cl_2, 0 °C to room temp, 95%; (2) Ac_2O, NEt_3, DMAP, CH_2Cl_2, 0 °C to room temp, 92%; (iv) $CH_2(CO_2Et)_2$, NaH, $Pd[PPh_3]_2Cl_2$, PPh_3, THF, 0 °C to room temp, 80%; (v) (1) H_2 (1 atm), Pd/C, CH_3OH, room temp; (2) 4-methoxybenzaldehyde, $NaBH(OAc)_3$, $AcOH_{cat}$, CH_2Cl_2, room temp, chromatographic separation, overall 72%; (vi) (1) Boc_2O, NEt_3, H_2O/THF, room temp; (2) $C_2H_5NO_2$, NaOEt, EtOH, −5 °C, 50%; (vii) (1) $MeNH_2$ (33 wt % in ethanol), room temp, 12 h, 70%; (2) CH_2Cl_2/TFA (4:1), 82%; (viii) H_2 (1 atm), PtO_2, CH_3OH, room temp, chromatographic separation 60%; (ix) (1) $C_2H_5NO_2$, NaOEt, EtOH, −5 °C, 76%; (2) $MeNH_2$ (33 wt % in ethanol), room temp, 84%.

Attempts to carry out the direct transformation of **38** into the corresponding oxime ester gave exclusively degradation of the starting material. Consequently, the amino group was protected with Boc_2O and compound **39** was then transformed into oxime amide **41** after deprotection.

Alternatively, double bond reduction with Pt_2O in MeOH was carried out in a mixture of **37a** and **37b**, giving the malonate **42** in 60% yield as a single isomer after column chromatography separation. On **42** the standard sequence of oximation and transformation of the ethyl ester into methylamide gave compound **43** in 84% isolated yields (Scheme 4). HPLC/MS analysis (Chiralpack column) and ^{19}F NMR analysis of the amides derived from **41** with (*S*)- and (*R*)-Mosher acids confirmed that racemization did not occur along the full synthetic pathway of chiral oxime amides (Scheme 4).

RESULTS AND DISCUSSION

HDAC Isoform Inhibition Assay. All the compounds prepared in this study were evaluated for their in vitro inhibitory activity against the 11 human HDACs isoforms in order to obtain a complete potency profile. The inhibitory activity was carried out as previously described using SAHA (**1**) as the reference compound.[17a,19]

dx.doi.org/10.1021/jm101373a |*J. Med. Chem.* 2011, 54, 2165–2182

Table 1. Activity of α-Oxime Amides against the 11 Human HDAC Isoforms (IC_{50}, μM)[a]

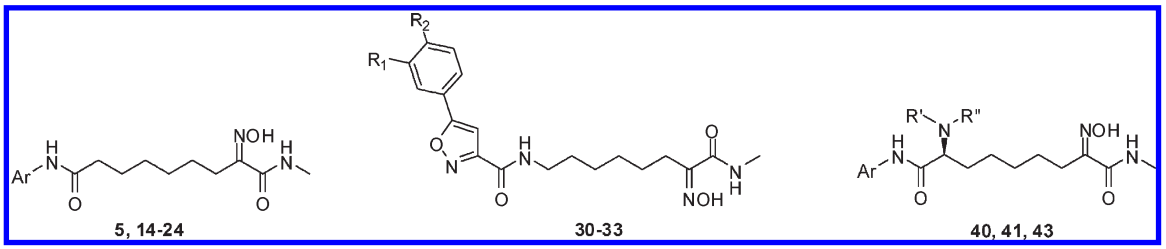

Entry	R'	R''	Ar	R_1	R_2	11 human HDAC isoforms (IC_{50}, μM)										
						1	2	3	4	5	6	7	8	9	10	11
SAHA		-	-	-	-	0.061	0.24	0.25	0.21	0.15	0.10	2.48	0.18	0.02	0.15	0.1
5	-	-	Ph	-	-	56.7	100	18.6	65.7	59.3	*	36.2	22.6	30.7	*	*
14	-	-		-	-	*	*	*	*	*	*	*	65.0	*	*	*
15	-	-		-	-	*	*	*	*	*	*	*	*	*	*	*
16	-	-		-	-	*	*	*	*	*	*	*	58.4	*	*	*
17	-	-	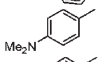	-	-	*	*	*	*	*	*	*	*	*	*	*
18	-	-	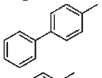	-	-	*	*	*	*	*	*	*	*	*	*	*
19	-	-		-	-	*	*	89.2	*	*	*	*	*	*	*	*
20	-	-	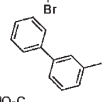	-	-	67.1	*	9.6	*	*	*	23.1	*	19.4	73.3	*
21	-	-	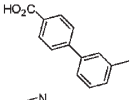	-	-	89.3	*	21.1	*	*	*	80.9	29.4	53.7	*	*
22	-	-	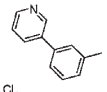	-	-	*	*	18.4	*	*	*	42.8	76.7	32.1	*	*
23	-	-	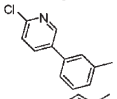	-	-	19.3	69.7	1.99	58.9	21.0	93.5	29.7	*	13.3	23.1	34.1
24	-	-	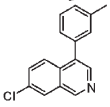	-	-	*	*	*	*	*	*	*	*	*	*	*
30	-	-	-	NHBoc	H	*	*	89.8	*	*	*	60.3	*	*	*	*
31	-	-	-	H	NHBoc	*	*	51.8	*	*	*	*	*	*	*	*
32	-	-	-	NH_2	H	8.12	33.0	1.88	38.9	13.0	*	5.25	*	2.55	15.4	16.8
33	-	-	-	H	NH_2	11.6	48.1	4.44	48.8	15.3	*	16.5	*	6.50	21.8	28.1
40	Boc	PMB	Ph	-	-	81.1	*	49.4	*	76.7	64.2	*	*	*	98.5	*
41	H	PMB	Ph	-	-	17.5	95.9	10.6	59.2	45.8	28.7	*	94.6	65.7	37.8	*
43	Bn	Bn	Ph	-	-	*	*	*	*	*	35.8	*	87.0	*	*	*

[a] The asterisk (*) represents IC_{50} > 100.

dx.doi.org/10.1021/jm101373a |J. Med. Chem. 2011, 54, 2165–2182

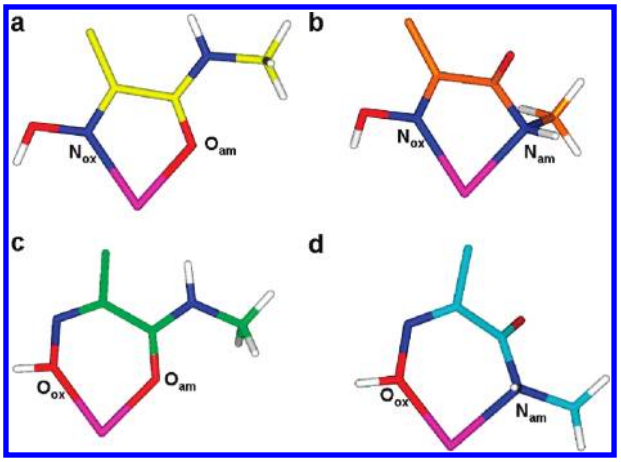

Figure 1. $5/Zn^{2+}$ complexes optimized at DFT level: (a) TC-NO complex; (b) TT-NN complex; (c) CC-OO complex; (d) CT-ON complex. Only zinc binding groups are shown for the sake of clarity. The conformers are colored by atom type [C = (a) yellow, (b) orange, (c) green, and (d) cyan; H = white; N = blue; O = red; Zn = magenta].

Table 2. Dihedral Angles and ZBG Distances of the α-Oxime Methylamide/Zn Complex

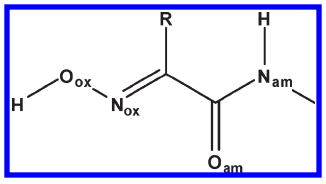

	τ_1 (deg)	τ_2 (deg)	D_1 (Å)	D_2 (Å)
		DFT		
TC-NO[a]	−0.37[b]	−1.29[c]	2.02[d]	2.23[e]
TT-NN[a]	−39.13[f]	7.74[c]	2.20[g]	2.22[e]
CC-OO[a]	32.17[b]	41.56[h]	2.00[d]	2.15[i]
CT-ON[a]	77.49[f]	18.95[h]	2.27[g]	2.15[i]
		Docking		
32[j]	1.75[b]	90.74[h]	2.63[d]	2.49[i]
32[k]	7.84[b]	17.00[c]	2.47[d]	2.99[e]
41	10.49[b]	86.73[h]	2.68[d]	2.49[i]

[a] DFT complexes as defined in the text and Figure 1. [b] $C_{ox}-C_{am}-O_{am}-Zn$ dihedral angle values. [c] $C_{am}-C_{ox}-N_{ox}-Zn$ dihedral angle values. [d] Distance between the O_{am} and Zn. [e] Distance between the N_{ox} and Zn. [f] $C_{ox}-C_{am}-N_{am}-Zn$ dihedral angle values. [g] Distance between N_{am} and Zn. [h] $C_{ox}-N_{ox}-O_{ox}-Zn$ dihedral angle values. [i] Distance between the O_{ox} and Zn. [j] First set of docking results. [k] Second set of docking results.

Structure−Activity Relationships (SARs). At first, compounds **2**−**5** (Chart 1) were tested to select a potentially new biasing binding element for the zinc in HDAC catalytic site (namely, ZBG). The α-keto oxime ester function of **2**, as well as the α-oxime ester of **3**, was inactive, while the comparison of the relative activities of compounds **4** and **5** indicated that the ability of the α-oxime amide function to inhibit HDAC catalytic site is related to the nature of the substituent on the amide nitrogen (Table 1). Interestingly, the same SAR trend was reported for a series of SAHA analogues characterized by the α-keto amide function as ZBG.[20] Since the HDAC natural substrate also contains an acetamide moiety, it is likely that a methyl substituted amide is able to reproduce substrate interaction with the catalytic site, thus leading to a gain of inhibitory activity (**4** vs **5**, Table 1). Although not comparable with SAHA, these data were encouraging, suggesting an effective binding of the α-oxime methylamide to the catalytic zinc. Consequently, with the aim of increasing inhibitory activity, different cap groups on the molecular skeleton of compound **5** were explored (**14**−**24**, Scheme 2). Some derivatives of this series showed increased activity against a number of HDAC isoforms (**20**−**23**, Table 1), even if their activity range is still far from the inhibition values of the reference compound. The shape of the steric hindrance around the phenyl ring was critical for inhibitory activity (compounds **14**−**19** and **24** vs compounds **20**−**23**, Table 1), while the presence of an acid or a basic substituent modulated activity (**23** > **20** > **22** > **21**, Table 1) and selectivity (**21**, **22** > **20** > **23**, Table 1). Still in the attempt to increase inhibitory activity, a Cap containing an arylisoxazole moiety was introduced (**30**−**33**, Scheme 3), as this modification has been described to generate very potent and selective hydroxamic acid inhibitors.[15] Compounds **30** and **31** carrying a hindered *N*-Boc group did not show any activity, whereas the *m*- and *p*-aniline derivatives **32** and **33** were more active, the former being the most active compound of the whole series. Thus, different from what was reported for their hydroxamic acid analogues,[15] the activity and the selectivity of compounds **30**−**33** were driven by the steric hindrance at the Cap region. Finally, to further explore SARs in the Cap, a stereogenic center carrying a nitrogen atom was introduced, leading to branched cap groups (**40**, **41**, and **43**; Scheme 4). Compound **41** still retained activity on HDACs 1, 3, and 9, while a wider loss of activity was again observed by further increasing the steric hindrance at the Cap, as in the case of the *N*-Boc derivative **40** and the bis-benzyl derivative **43** (Table 1).

Thus, in the search of new ZBGs, the α-oxime amide function on one hand showed an overall poorer ability to fulfill HDAC catalytic site pharmacophore compared to hydroxamic acid. On the other hand, it conferred to our compounds a peculiar paralogue selectivity profile. In order to rationalize these somehow contradictory results in terms of HDAC activity and selectivity, a computational approach was carried out.

Computational Studies. The accommodation of the ZBG into the HDAC catalytic site is a crucial step of the inhibition process and is finely controlled by its zinc coordination ability and by key interactions with the surrounding protein residues. First, we analyzed the ability of the α-oxime amide function to coordinate the zinc atom by using a computational protocol, which included a dynamic (SA) conformational search followed by molecular mechanic (MM) and semiempirical (PM6) geometry optimization to generate input structures for calculations at the density functional theory (DFT) level (see Experimental Section for details). Our results indicated the putative formation of several zinc coordination complexes, involving different α-oxime amide heteroatoms. In particular, our analysis identified four putative complexes, two of which were characterized by a five-membered metal coordination ring and two by a six-membered metal coordination ring, named according to their $O_{ox}-N_{ox}-C_{ox}-C_{am}$ and $O_{am}-C_{am}-C_{ox}-N_{ox}$ dihedral angles values ($C = 0°$; $T = 180°$) and zinc coordination atoms (NO = Nox and Oam; NN = Nox and Nam; OO = Oox and Oam; ON = Oox and Nam) (Figure 1, Table 2).

dx.doi.org/10.1021/jm101373a |*J. Med. Chem.* 2011, 54, 2165–2182

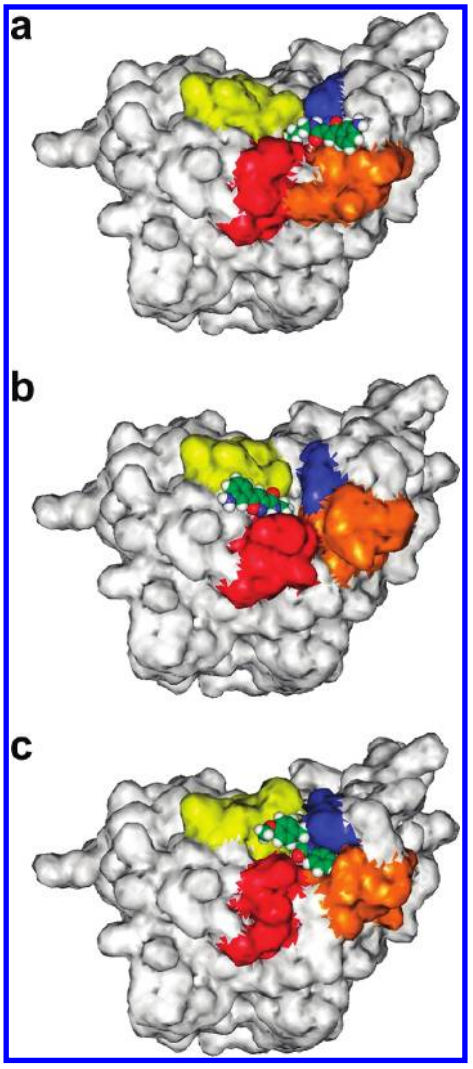

Figure 2. Overall view of HDAC 7 in complex with compound **32** [binding mode 1 (a) and binding mode 2 (b)] and compound **41** (c). vdW volumes of the ligands (colored in green) are displayed. Connolly surface of the enzyme is shown and colored on the base of active site substructures. The region V623−I628 (blue) and loop H732−S741 (yellow) set up pocket 1. Loop H732−S741 (yellow) and the region E804-G812 (red) set up pocket 2. The region H531−H544 (orange) and region E804-G812 (red) set up pocket 3.

All structures presented a planar coordination geometry in which the atoms involved in zinc coordination tend to lie on the same plane of the metal. A fragment based search was performed in the Cambridge Structural Database (CSD) using as query an α-oxime amide function in complex with zinc, and the structural analysis of the results (CSD codes BICFUP, CABTUU, GIFSAF, GEPMET, IXEBIW, LOVQUI, MEHZUU, WASXEV, ZUDLUF) confirmed our computational data. Thus, starting from the calculated zinc coordination geometries (Figure 1), compounds **32** and **41** were introduced into the human HDAC 7 (PDB code 3C0Y) active site and several dynamic docking procedures were carried out considering either a bi- or a monodentate zinc interaction mode. In particular, (a) a six-membered bidentate O−O interaction mode, (b) a monodentate interaction mode by the amide oxygen, and (c) a monodentate interaction mode by the oxime oxygen were considered for the CC-OO DFT conformer, and (d) a five-membered bidentate N−N interaction mode, (e) a monodentate interaction mode by the oxime nitrogen, and (f) a monodentate interaction mode by the amide nitrogen were considered for the TT-NN DFT conformer (see Experimental Section for details). All the other DFT conformers (Figure 1, Table 2) when inserted in the enzyme catalytic site caused a steric clash with enzyme residues and/or zinc. Each of the six docking starting structures produced 20 results, which were selected on the bases of inhibitor conformations (solutions presenting cis alkyl chain or amide bond were discarded) and grouped according to enzyme−inhibitor interactions. In particular, the coordination geometry of the ZBG and the positions of (i) the hydroxyl group, (ii) the methyl group, (iii) the alkyl chain, (iv) the H-bond group at the end of the alkyl chain, and (v) the aromatic Cap have been analyzed and compared to those reported in all known inhibitors/HDAC X-ray complexes present in the Brookhaven PDB (Table 2SI in the Supporting information). This analysis provided an explanation for the inhibitory activity profile of our α-oxime amide derivatives on classes I and IIa HDAC enzymes.

Compound **32** produced two main sets of results (Figures 2a,b and 3a,b). In the first set of docking results (binding mode 1, Figures 2a and 3a) the ZBG binds His669 through its hydroxyl hydrogen and interacts with the zinc atom through the amide oxygen and the oxime oxygen, thus forming a six-membered metal coordination ring. The resulting coordination geometry is very different from that calculated through DFT methods (CC-OO complex, Figure 1, Table 2), revealing a reduced zinc binding ability of the α-oxime amide function when introduced into HDAC catalytic site. The *N*-methylamide group reproduces trifluoromethyl ketone (TFMK, PDB code 2VQJ; Table 2SI in the Supporting information) interactions with Pro667, Gly678, Phe679, and Gly841 (human HDAC 7 numbering), while the volume of the aliphatic linker occupies a region similar to that covered by X-ray determined inhibitors in complex with HDAC (Figure 3a, Table 2SI in the Supporting information). Finally, the amide function at the end of the linker interacts with Thr625 through its nitrogen and the aromatic cap group is surrounded by Cys535, Asp537, Pro617, Cys618 (structural Zn coordination site; Figures 2a and 3a).

The second set of docking results obtained for compound **32** (binding mode 2, Figures 2b and 3b) still presents the *N*-methylamide group positioned in the same enzyme cleft occupied by TFMK (Table 2SI in the Supporting information), as occurred for binding mode 1. Nevertheless, the α-oxime amide function is differently oriented with the hydroxyl hydrogen binding Asp801 and the amide oxygen and oxime nitrogen interacting with zinc through a five-membered ring coordination geometry (Figure 3b). In this case, the docked structure is similar to the one obtained by DFT calculations (TC-NO complex, Figure 1) even if, because of the presence of the protein Zn coordinators, it showed an increased distance between the oxime nitrogen and the zinc atom (D2, Table 2). The aromatic amide function at the end of the linker interacts through an H-bond with the backbone of Ala808, while the Cap is positioned within the region Asp801-Gly812 and loop Arg731-Pro739 (named pocket 2 in Figure 2b). A comparison of this set of docking results with X-ray determined HDAC inhibitor structures (Table 2SI in the Supporting information) revealed that the only X-ray determined HDAC complex in which the ligand projects the cap region in pocket 2 (Figure 2) is that of APHA in complex with HDAC 8 (PDB code 3F07). All the other cocrystallized ligands

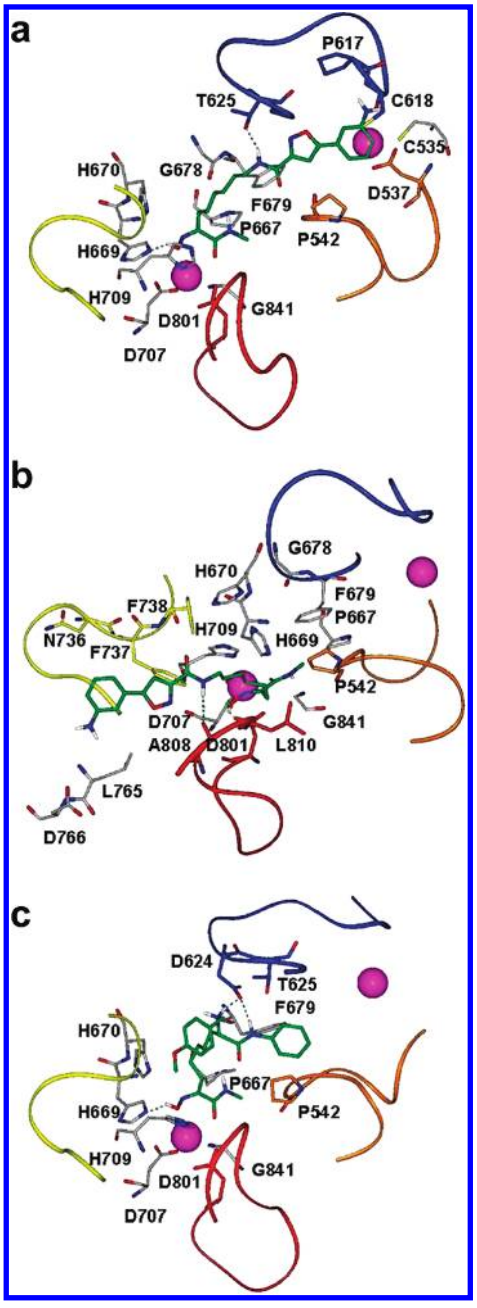

Figure 3. (a) Binding mode 1 of **32** in HDAC 7. (b) Binding mode 2 of **32** in HDAC 7. (c) Docked complex of **41**/HDAC 7. HDAC 7 active site substructures are colored: orange (D537-R547); blue (P617-T627); yellow (loop R731-P739); red (D801-G812). Carbon atoms of the ligands are colored in green. vdW volumes of catalytic and structural zinc (magenta) are displayed. Heteroatoms are colored by atom type (O = red; N = blue). Hydrogen bonds are highlighted by green dashed lines. Hydrogens and water molecules are omitted for clarity except those involved in hydrogen bond interactions.

occupy the regions between loop Arg731-Pro739 and region Pro617-Thr627 (human HDAC 7 numbering; pocket 1 in Figure 2) and/or between loop region Asp537-Arg547 and loop Asp801-Gly812 (human HDAC 7 numbering; pocket 3 in Figure 2). Interestingly, similar to **32**, APHA is characterized by a lower (i.e., in the micromolar range) in vitro HDAC inhibition constant[21] compared to other classes of known inhibitors, including SAHA. Thus, with adoption of binding

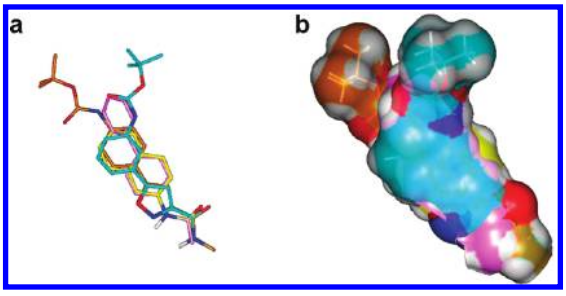

Figure 4. Superimposition of cap groups of low energy conformers of **14** (yellow), **18** (pink), **30** (cyan), and **31** (orange) by fitting the carbonyl group atoms and the amide and isoxazole nitrogens. Structures are displayed as sticks (a) and as Connolly surfaces (b). In (a) all hydrogens, except those of amide function, have been omitted for the sake of clarity.

mode 2, the α-oxime amide function is better accommodated in the catalytic site. However, the volume of the alkyl chain of **32** does not fit the volume occupied by any ligand cocrystallized in complex with HDAC (Figure 2b, Table 2SI in the Supporting information), thus projecting the Cap in a surface pocket different from that occupied by SAHA and accounting for the peculiar SARs and selectivity profile of the α-oxime amide derivatives. Indeed, the oxazole ring of **32** is involved in $\pi-\pi$ interaction with Phe737 (loop Arg731-Pro739) and the aniline moiety is embedded between Asn736 and Leu765, Asp766 (loop Gly763-Pro767) (Figure 3b). The side chains of Leu765 and Asp766 surround the aromatic amine, thus explaining the inactivity of sterically hindered derivatives, such as **30** and **31** (Scheme 3, Table 1). The presence of the bulky Met274 in HDAC 8 (Table 3SI in the Supporting information), replacing HDAC 7 Leu810 (Figure 3b), may account for the inactivity of **32** against this HDAC isoform. Indeed, the less hindered monophenyl analogue **5** resulted the most active derivative of the series on HDAC 8 (Table 1). The structural superimposition of low energy conformers of **5** and **14**−**24** on low energy conformers of **30**−**33** pointed out that the steric bulk that unfavorably affects their HDAC inhibitory activity (**14**−**19**, **24** vs **5**, **20**−**23**; **30**, **31** vs **32** and **33**; Table 1) partially overlays (Figure 4), suggesting a similar binding mode for the two series of compounds.

In this view, the complete loss of activity of compound **21** bearing a *p*-carboxylic function on the phenyl ring (Scheme 2, Table 1) is in agreement with the presence of a negatively charged residue (Asp766) on the loop Gly763-Gly770, conserved in all HDAC isoforms (Table 3SI and Figure 2SI in the Supporting Information). Moreover, the activity of the monophenyl derivative **5** toward HDAC 3 could be explained by the different amino acid composition of pocket 2 (Figure 2b). Indeed, only HDAC 3 presents an additional aromatic residue in this region (Tyr198, human HDAC 3 numbering), which, replacing HDAC 7 Asn736 (Figure 3b), could establish favorable $\pi-\pi$ interactions with the phenyl ring of **5**. On the contrary, all other HDAC isoforms lack residues able to interact with the Cap of **5** (Table 3SI in the Supporting information).

In the case of compound **41** all input structures led to only one set of docking results (Figures 2c and 3c). Compared to **32** compound **41** loses activity against HDAC 7, accordingly; the strong (ionic) interaction between the protonated nitrogen at the Cap level and Asp624 in region Pro617-Thr627 (loop 2, Figure 2c) seems to drive enzyme binding, inducing a distortion

in **41** alkyl chain conformation and reducing ZBG accommodation in the catalytic site. The zinc atom in the catalytic site is coordinated through the amide oxygen and the oxime oxygen, as in the case of binding mode 1 of **32**, presenting a six-membered metal coordination geometry, which was very different from that calculated through DFT methods (CC-OO complex, Figure 1, Table 2). The amide methyl group of **41** accommodates in the cleft formed by Pro667, Phe679, and Gly841, reproducing HDAC cocrystallized ligand positioning, as was also for compound **32** in both sets of docking results. Moreover, the threonine residue present in HDAC 7 (Thr625) on loop 2, just after Asp624, hinders the accommodation of the branched cap group of **41**. This residue is replaced by a negatively charged residue in HDACs 1 and 3 (Glu98 and Asp92, respectively). This could account for the higher inhibitory activity of **41** toward these enzyme isoforms and for the complete lack of activity of compounds **40** and **43**, bearing a bulky *N*-Boc group and a benzyl group on the amine nitrogen, respectively (Scheme 4, Table 1). The *p*-OMe phenyl ring is accommodated in the same region (pocket 2 in Figure 2c) occupied by the **32** cap group in the second set of docking results (Figure 2b). On the other hand, the phenyl ring of **41** interacts with region Asp537-Arg547 (loop 1; Figures 2c and 3c) similar to **32** Cap, according to the binding mode obtained in the first set of docking results (Figure 2a).

The hypothesized binding modes also relate with the low activity of all our derivatives toward HDAC 8. Indeed, in this isoform, HDAC 7 Pro667 and Pro542 (Figure 3) are replaced by Trp141 and Lys33, respectively (Table 3SI in the Supporting information), thus preventing the accommodation of the α-oxime amide group in the catalytic site. On the other hand, the lack of activity against HDAC 4 can be due to the presence of Pro809, corresponding to Ala676 in HDAC 7 (Table 3SI in the Supporting information), which limits the structural flexibility of a loop undergoing a significant conformational change during our docking calculations (Ala676-Cys680 loop, rms value on all Cα atoms of 2.6 Å).

In summary, our computational results illustrated how the α-oxime amide moiety scarcely adapts into HDAC catalytic site, being not able to reproduce any known Zn binding mode except for the position of the amide methyl group, which indeed was critical for the inhibitory activity (**4** vs **5**, Table 1). The positioning of the ZBG affects the placement of the Cap on the enzyme surface pockets, whose different amino acid composition among HDAC isoforms is mainly responsible for inhibitor selectivity. Accordingly, the introduced modifications at the Cap of our α-oxime amide derivatives did not produce the same HDAC inhibitor profile reported for their hydroxamic acid analogues.

The rationalization of the peculiar binding profile of oxime derivatives provides us with a useful tool to continue our investigation on HDAC inhibitors. Indeed, the information on the mutual relation between ZBG and Cap positioning will be exploited to sample the enzyme pockets at the entrance of the channel where isoform selectivity stands. Moreover, our study disclosed interesting insights into the molecular determinants for ZBG accommodation into the catalytic site, which will be further explored through the synthesis of new optimized derivatives.

CONCLUSIONS

Adopting a different binding mode with respect to that reported for hydroxamic acid and substrate-like HDAC inhibitors, α-oxime amide derivatives show in vitro inhibitory activity in the micromolar range and a peculiar paralogue selectivity profile. Different from results observed for some class I selective inhibitors, our α-oxime amides do not select between class I and class II HDAC; rather they target specific isoforms in each class. Our computational results indicate that despite its ability to coordinate the zinc ion, the α-oxime amide function of compounds **32** and **41** was able to reproduce known inhibitor−substrate ZBG interactions with the HDAC catalytic site. The unusual accommodation of the ZBG was also critical for the positioning of the linker and the projection of the Cap toward the different surface pockets of the enzyme. Accordingly, the SARs of the new derivatives differ from those of other classes of active compounds. The rationalization of the activity profile of the new oxime amide derivatives lays the base for future structural modifications.

EXPERIMENTAL SECTION

Chemistry. Reagents were purchased from commercial suppliers and used without further purification. Anhydrous reactions were run under (a positive pressure) dry N_2. Flash chromatography employed Merck silica gel 60 (23−400 mesh). Microwave dielectric heating was applied using a CEM Discover microwave oven for chemical synthesis. NMR spectra were acquired at 300 K using Bruker AC200F and Bruker Advance DPX400 spectrometers. Data are reported as chemical shifts (δ ppm), multiplicity (s = singlet, bs = broad singlet, d = doublet, dd = doublet of doublets, t = triplet, m = multiplet), coupling constants (J, Hz), and relative integral. Chemical shifts are reported relative to tetramethylsilane at 0.00 ppm. Mass spectral (MS) data were obtained using an Agilent 1100 LC/MSD VL system (G1946C) with a 0.4 mL/min flow rate using a binary solvent system of 95:5 methanol/water. UV detection was monitored at 254 nm. Mass spectra were acquired either in positive or in negative mode scanning over the mass range of 105−1500. Microwave irradiations were conducted using a CEM Discover synthesis unit (CEM Corp., Matthews, NC). Elemental analyses were performed on a Perkin-Elmer PE 2004 elemental analyzer, and the data for C, H, and N are within 0.4% of the theoretical values. The chemical purity of the target compounds was determined using the following conditions: an Agilent 1100 series LC/MS with a EC 125/4.6 NUCLEODUR 100-5 C18 reversed phase column. The binary solvent system (A/B) was as follows: 0.1% TFA in water (A) and acetonitrile (B). The absorbance was detected at 254 nm, and the flow rate was 1 mL/min. The purity of each compound was ≥95% in either analysis.

Ethyl 2-(Hydroxyimino)-3,10-dioxo-10-(phenylamino)decanoate (2). β-Keto ester **8** (0.207 g, 0.649 mmol) was dissolved in glacial acetic acid (5 mL) and cooled to 0 °C in ice bath. A solution of $NaNO_2$ (0.089 g, 1.30 mmol) in H_2O (2 mL) was added. The reaction mixture was allowed to warm to room temperature and stirred overnight. Dry Et_2O was added, and the organic layer was separated, washed with saturated $NaHCO_3$, dried (anhydrous Na_2SO_4), filtered, and concentrated in vacuo. The crude residue was purified by flash chromatography (99:1 dichloromethane/methanol) to afford the title compound **2** as a colorless oil (0.180 g, 80%). ^{1}H NMR (400 MHz, $CDCl_3$): δ 1.3 (t, J = 6.8 Hz, 3H), 1.34 (m, 4H), 1.59 (m, 2H), 1.72 (m, 2H), 2.3 (t, J = 7.6 Hz, 2H), 2.71 (t, J = 6.8 Hz, 2H), 4.31 (q, J = 7.2 Hz, 2H), 7.05 (t, J= 8.8 Hz, 1H), 7.25 (m, 2H), 7.5 (2H, J = 8 Hz, 2H). MS(ESI) m/z: 371.1 $[M + Na]^+$. Anal. Calcd for $C_{18}H_{24}N_2O_5$: C, 63.73; H, 7.55; N, 8.74. Found: C, 63.93; H, 7.49; N, 8.69.

General Procedure To Convert Alkylated Malonic Ester to α-Oxime Ester. Ethyl 2-(Hydeoxyimino)-9-oxo-9, 8-phenylamino)nonanoate (3). Diester **13** (0.473 g, 1.30 mmol) was placed in a 50 mL flask equipped with a magnetic stirring bar and N_2 inlet. The

flask was immersed in an ice bath, and a solution of ethyl nitrite in ethanol (1.31 mL, 2.61 mmol) was added to the stirred solution. The mixture was then cooled to −5 °C in ice−salt bath, and 1.31 mmol of sodium ethoxide (prepared from 0.030 g of sodium in 2 mL of dry ethanol) was added slowly with stirring. The resulting reaction mixture was allowed to warm to room temperatue during the night. The solvent was concentrated under reduced pressure. To the residue equal volumes of ice−water and cold concentrated hydrochloric acid were added until pH 4 was obtained. The aqueous solution was extracted three times with diethyl ether. The combined ether extracts were dried (anhydrous Na_2SO_4), filtered, and evaporated to dryness. The crude was purified by flash chromatography (100% dichloromethane) to afford the title compound **3** as a white solid (0.384 g, 92%). Mp 118−120 °C. ^{1}H NMR (400 MHz, $CDCl_3$): δ 1.3 (t, J = 7.2 Hz, 3H), 1.35 (m, 4H), 1.52 (m, 2H), 1.70 (m, 2H), 2.32 (t, J = 3.8 Hz, 2H), 2.59 (t, J = 7.2 Hz, 2H), 4.28 (q, J = 7.2 Hz, 2H), 7.05 (t, J = 8.8 Hz, 1H), 7.25 (m, 2H), 7.5 (d, J = 8 Hz, 2H). MS(ESI) m/z: 343.1 $[M + Na]^+$. Anal. Calcd for $C_{17}H_{24}N_2O_4$: C, 63.73; H, 7.55; N, 8.74. Found: C, 63.79; H, 7.51; N, 8.70.

8-(Hydroxyimino)-*N*^{1}-phenylnonanediamide (4). To a solution of **3** (0.050 g, 0.16 mmol) in ammonium hydroxide solution (28−30%, 5 mL) a catalytic amount of ammonium chloride was added. The resulting mixture was stirred at room temperature for 18 h. The reaction mixture was diluted with ethyl acetate, and the organic layer was separated, dried (anhydrous Na_2SO_4), filtered, and concentrated in vacuo. The crude was purified by flash chromatography (ethyl acetate/petroleum ether 6:4) to afford the desired compound **4** as a yellow solid (0.042 g, 90%). Mp 134−136 °C. ^{1}H NMR (400 MHz, CD_3OD): δ 1.36 (m, 4H), 1.48 (m, 2H), 1.66 (m, 2H), 2.32 (t, J = 3.8 Hz, 2H), 2.52 (t, J = 7.2 Hz, 2H), 7.05 (t, J = 8.8 Hz, 1H), 7.25 (m, 2H), 7.5 (d, J = 8 Hz, 2H). MS(ESI) m/z: 314.1 $[M + Na]^+$. Anal. Calcd for $C_{15}H_{21}N_3O_3$: C, 61.84; H, 7.27; N, 14.42. Found C, 61.79; H, 7.23; N, 14.40.

General Procedure To Convert the Oximino Ester to α-Oxime Amide. 2-(Hydroxyimino)-*N*^{1}-methyl-*N*^{9}-phenylnonanediamide (5). Compound **3** (0.170 g, 0.302 mmol) was dissolved in 7 mL of methylamine solution (33 wt % in ethanol), and the reaction mixture was stirred at room temperature overnight. The solvent was evaporated to dryness and the residue purified by flash chromatography (dichloromethane/methanol 95:5) to afford the desired compound **5** as a white solid (0.074 g, 80%). Mp 138−140 °C. ^{1}H NMR (200 MHz, $CDCl_3$): δ 1.34 (m, 4H), 1.50 (m, 2H) 1.72 (m, 2H), 2.24 (t, J = 6.8 Hz, 2H), 2.7 (t, J = 7.2 Hz, 2H), 2.75 (s, 3H), 7.03 (t, J = 8.8 Hz, 1H), 7.13 (m, 2H), 7.48 (d, J = 8 Hz, 2H). MS(ESI) m/z: 328.2 $[M + Na]^+$. Anal. Calcd for $C_{16}H_{23}N_3O_3$: C, 62.93; H, 7.59; N, 13.76. Found: C, 62.88; H, 7.55; N, 13.73.

8-Oxo-8-(phenylamino)octanoic Acid (7). Acetic anhydride (25 mL) was placed in a 250 mL flask equipped with a magnetic stirrer and a refrigerator and warmed to 180 °C. While the mixture was refluxing, suberic acid (10 g, 57 mmol) was added. The resulting solution was warmed for 2 h and then concentrated. After concentration, the product was crystallized from DCM. After drying the product weighed 3.1 g and a second crop was obtained from the mother liquor to obtain the intermediate anhydride in 39% of combined yield. To a solution of acetylated suberic acid in anhydrous THF (20 mL) was added aniline (0.56 mL, 6.2 mmol) at room temperature. The reaction mixture was stirred for 2 h and then treated with 150 mL of H_2O and 3 g of K_2CO_3. The basic resulting aqueous solution was stirred for 20 min and then extracted three times with EtOAc. The combined organic phases contained only the secondary product bis-anilide, whereas the aqueous phase was treated with HCl until pH 3−4 was obtained. The monoanilide **7**, precipitating during the night at 4 °C, was filtered and dried over P_2O_5 (74% yield, the product is a white solid). Mp 114−116 °C. ^{1}H NMR (200 MHz, $CDCl_3$): δ 1.29 (m, 4H), 1.55 (m, 2H), 1.65 (m, 2H), 2.30 (t, J = 3.8 Hz, 2H), 2.35 (t, J = 3.8 Hz, 2H), 7.05 (t, J = 8.8 Hz, 1H), 7.25 (m, 2H), 7.5 (d, J = 8.0 Hz, 2H). MS(ESI) m/z: 272.1 $[M + Na]^+$. Anal. Calcd for $C_{14}H_{19}NO_3$: C, 67.45; H, 7.68; N, 5.62. Found: C, 67.40; H, 7.65; N, 5.60.

Ethyl 3,10-Dioxo-10-(phenylamino)decanoate (8). To a solution of **7** (1.08 g, 4.36 mmol) in anhydrous THF (25 mL) was added carbonyldiimidazole (0.777 g, 4.79 mmol) at room temperature. The reaction mixture was stirred for 6 h. Magnesium salt of monoethyl malonate (prepared from 4.03 g of monoethyl malonate and 1.74 g of $Mg(OEt)_2$) was added, and the resulting mixture was stirred overnight. After concentration under reduced pressure, the residue was purified by flash chromatography (petroleum ether/diethyl ether 1:9) to afford **8** (1.27 g, 91%) as a colorless oil. ^{1}H NMR (400 MHz, $CDCl_3$): δ 1.25 (t, J = 6.8 Hz, 3H), 1.34 (m, 4H), 1.58 (m, 2H), 1.68 (m, 2H), 2.3 (t, J = 7.6 Hz, 2H), 2.49 (t, J = 6.8 Hz, 2H), 3.4 (s, 2H), 4.15 (q, J = 7.2 Hz, 2H), 7.05 (t, J = 8.8 Hz, 1H), 7.25 (m, 2H), 7.5 (d, J = 8 Hz, 2H). MS(ESI) m/z: 342.1 $[M + Na]^+$. Anal. Calcd for $C_{18}H_{25}NO_4$: C, 67.69; H, 7.89; N, 4.39. Found: C, 67.72; H, 7.84; N, 4.34.

Benzyl 7-Iodoheptanoate (10). To a solution of ethyl 7-bromoheptanoate (1.3 g, 6.3 mmol) in THF/H_2O/EtOH 1:1:1 (15 mL), LiOH (0.343 g, 8.19 mmol) was added. The reaction mixture was stirred for 3 h. The solvent was removed, and the residue was dissolved in CH_2Cl_2. The reaction mixture was acidified with 4 M HCl until pH 1 was obtained. The organic layer was separated, washed with $NaCl_{ss}$, dried over sodium sulfate, filtered, and concentrated in vacuo. The crude was submitted to the next step without additional purification (98%). The crude 7-bromoheptanoic acid (1.3 g, 6.3 mmol) and DMAP (0.077 g, 0.63 mmol) were then added to a solution of benzyl alcohol (1.3 mL, 12.6 mmol) and EDC (2.4 g, 12.6 mmol) in CH_2Cl_2 (3 mL) at 0 °C. The resulting mixture was stirred at room temperature for 7 h. Then it was poured into water and extracted with CH_2Cl_2 × 3. The organic layer was washed with saturated aqueous $NaHCO_3$ × 2, water, and brine, dried (anhydrous Na_2SO_4), filtered, and concentrated. The crude was purified by flash column chromatography (petroleum ether/ethyl acetate 9:1) to afford the benzyl 7-bromoheptanoate as a colorless oil (91%). A solution of this bromide (0.3 g, 1.0 mmol) in acetone (1 mL) was added to a solution of NaI (0.45 g, 3.01 mmol) in acetone (1 mL), and the resulting mixture was stirred overnight (18 h) at room temperature. The precipitate NaBr was filtered off, and the filtrate was concentrated under reduced pressure. The pulpy yellow residue was purified by flash chromatography (petroleum ether/ethyl acetate 9:1) to yield iodide **10** (0.336 g, 97%) as a colorless oil. ^{1}H NMR (400 MHz, $CDCl_3$): δ 1.49−1.22 (m, 4H), 1.70−1.55 (m, 4H), 2.29 (t, J = 7.6 Hz, 2H), 3.41 (t, J = 6.8 Hz, 2H), 5.06 (s, 2H), 7.29−7.24 (m, 5H). ^{13}C NMR (100 MHz, $CDCl_3$): δ 24.3, 26.0, 27.8, 33.9, 33.6, 44.4, 65.5, 127.7 (×3), 128.05 (×2), 135.8, 172.6. MS(ESI) m/z: 368.7 $[M + Na]^+$

7-Benzyl 1,1-Diethylheptane-1,1,1-tricarboxylate (11). NaH (1.05 g, 26.2 mmol, 60% dispersion in oil) was added to a two-necked round-bottom flask closed with a septum to which dry hexane (4 mL) was added, and the mixture was stirred for 5 min to dissolve the mineral oil. The hexane was removed by a syringe, THF (10 mL) was added, and the resulting mixture was stirred at 0 °C for 15 min. A solution of diethyl malonate (6.7 mL, 44 mmol) in THF (12 mL) was then slowly added over 30 min at 0 °C to the resulting suspension. The solution became clear after 10 min of stirring. The stirring was continued for another 30 min. Iodide **10** (5.05 g, 14.6 mmol) in THF (15 mL) was added dropwise over 30 min to the stirred solution, and this mixture was stirred at room temperature for 4 h. The reaction mixture was quenched with NH_4Cl_{ss}. The aqueous phase was extracted three times with ether, and the combined organic phases were dried (anhydrous Na_2SO_4), filtered and evaporated in vacuo. The crude residue was purified by flash chromatography (hexanes/ethyl acetate 9:1) to afford **11** as a colorless oil (4.84 g, 88%). ^{1}H NMR (200 MHz, $CDCl_3$): δ 1.23 (t, J = 6.9 Hz, 6H), 1.30 (m, 4H), 1.7 (m, 4H), 1.87 (m, 2H), 2.3 (t, J = 3.8 Hz, 2H), 3.30 (t, J = 7.2 Hz, 1H), 4.20 (q, J = 6.8 Hz, 4H), 5.09 (s, 2H), 7.05 (t, J =

8.8 Hz, 1H), 7.25 (m, 2H), 7.5 (d, J =8.0 Hz, 2H). ^{13}C NMR (50 MHz, $CDCl_3$): δ 13.7, 24.5, 26.9, 28.3, 28.4, 28.5, 33.8, 41.3, 51.6, 60.9 (×2), 61.1, 65.7, 127.6, 127.6, 128.2, 135.6, 166.3, 169.1 (×2), 173.1. MS(ESI) m/z: 386.1 $[M + Na]^+$. Anal. Calcd for $C_{21}H_{30}O_6$: C, 66.65; H, 7.99. Found: C, 66.60; H, 7.95.

9-Ethoxy-8-(ethoxycarbonyl)-9-oxononanoic Acid (12). Pd−C (0.32 g, 10% in mmol, 10% w/w) was added to a solution of **11** (0.993 g, 2.6 mmol) in $CHCl_3$ (30 mL), and the mixture was stirred under H_2 (1 bar) for 15 h. After full conversion, the reaction mixture was filtered and concentrated in vacuo. Flash chromatography (petroleum ether/ethyl acetate 7:3) gave **12** (96%) as a colorless oil. ^{1}H NMR (400 MHz, $CDCl_3$): δ 1.21 (t, J = 7.2 Hz, 6H), 1.57 (m, 2H), 1.29 (m, 6H), 1.83−1.82 (m, 2H), 2.28 (t, J = 7.2 Hz, 2H), 3.25 (t, J = 7.6 Hz, 1H), 4.15 (q, J = 7.2 Hz, 4H). ^{13}CNMR (100 MHz, $CDCl_3$) δ: 13.6 (×2), 24.0, 26.6, 28.2, 28.2, 28.4, 33.5, 51.5, 60.8 (×2), 169.1 (×2), 179.5. MS(ESI) m/z: 310.8 $[M + Na]^+$. Anal. Calcd for $C_{14}H_{24}O_6$: C, 58.32; H, 8.39. Found: C, 58.27; H, 8.35.

General Amidation Reaction Procedure via Acyl Chloride Intermediate. Diethyl 2-(7-Oxo-7-(phenylamino)heptyl)malonate (13). To a suspension of **12** (0.3 g, 1.04 mmol) in CH_2Cl_2 (2.5 mL) were added oxalyl chloride (0.13 mL, 1.5 mmol) and a catalytic amount of DMF. The mixture was stirred at room temperature for 2 h. The solvent was removed by evaporation in vacuo to give acid chloride intermediate. A solution of this chloride in CH_2Cl_2 (1.3 mL) was added dropwise to a solution of aniline (0.53 g, 5.7 mmol) and triethylamine (0.43 mL, 3.12 mmol) in CH_2Cl_2 (3.2 mL) cooled in an ice−water bath. The mixture was stirred at room temperature for 18 h. Then it was diluted with CH_2Cl_2 and washed with HCl 1 M, water, and brine, before being dried over anhydrous Na_2SO_4. Filtration and concentration in vacuo and purification by flash chromatography (petroleum ether/ethyl acetate 8:2) gave the title compound **13** as a white solid (80%). Mp 65−67 °C. ^{1}H NMR (400 MHz, $CDCl_3$): δ 1.23 (t, J = 6.8 Hz, 6H), 1.33 (m, 6H), 1.67 (m, 2H), 1.85 (m, 2H), 2.28 (t, J = 7.2 Hz, 2H), 3.27 (t, J = 7.2 Hz, 1H), 4.14 (q, J = 6.8 Hz, 4H), 7.04 (m, 1H), 7.24 (t, J = 7.6 Hz, 2H), 7.48 (d, J = 8.0 Hz, 2H), 7.68 (bs, 1H). ^{13}C NMR (100 MHz, $CDCl_3$): δ 14.06 (×2), 25.2, 26.9, 29.1, 28.5, 28.7, 37.3, 51.9, 61.3 (×2), 119.9 (×2), 124.0, 128.9 (×2), 138.1, 169.5 (×2), 171.5. MS(ESI) m/z: 371.8 $[M + Na]^+$. Anal. Calcd for $C_{20}H_{29}NO_5$: C, 66.09; H, 8.04; N, 3.85. Found: C, 66.01; H, 8.00; N, 3.83.

2-(Hydroxyimino)-*N*^{1}-methyl-*N*^{9}-(naphthalene-2-yl)nonanediamide (14). Compound **14** was prepared from the corresponding α-oxime ester using the procedure described for **5** in 76% yield as a yellow solid. Mp 153−155 °C. ^{1}H NMR (400 MHz, CD_3OD): δ 1.57−1.23 (m, 9H), 1.72−1.67 (m, 2H), 2.39 (t, J = 7.2 Hz, 2H), 2.54 (t, J = 7.6 Hz, 2H), 2.75 (s, 3H), 7.42−7.30 (m, 2H), 7.52 (d, J = 8.8 Hz, 1H), 7.77−7.72 (m, 3H), 8.17 (s, 1H). ^{13}C NMR (50 MHz, CD_3OD): δ 22.4, 24.5, 24.9, 25.0, 28.1, 28.5, 28.7, 36.2, 115.9, 119.4, 123.9, 125.4, 126.6, 127.5, 129.9, 133.2, 135.3, 153.1, 165.0, 172.9. MS(ESI) m/z: 355.8 $[M + H]^+$. Anal. Calcd for $C_{20}H_{25}N_3O_3$: C, 67.58; H, 7.09; N, 11.82. Found: C, 67.50; H, 7.04; N, 11.80.

2-(Hydroxyimino)-*N*^{1}-methyl-*N*^{9}-(quinolin-3-yl)nonanediamide (15). Compound **15** was prepared from the corresponding α-oxime ester using the procedure described for **5** in 80% yield as a white solid. Mp 208−210 °C. ^{1}H NMR (400 MHz, CD_3OD): δ 1.22 (m, 4H), 1.34 (m, 2H), 1.57 (m, 2H), 2.26 (t, J = 7.2 Hz, 2H), 2.39 (t, J = 7.6 Hz, 2H), 2.64 (s, 3H), 7.36 (t, J = 7.6 Hz, 1H), 7.45 (t, J = 6.8 Hz, 1H), 7.63 (d, J = 8 Hz, 1H), 7.79 (d, J = 8.4 Hz, 1H), 8.61 (bs, 2H). ^{13}C NMR (50 MHz; $CDCl_3$): δ 22.9, 25.1, 25.4 (×2), 28.4, 28.9, 36.7, 124.1, 127.0, 127.5 (×2), 128.1, 128.2, 132.3, 143.7, 143.8, 153.7, 164.9, 173.6. MS(ESI) m/z: 378.8 $[M + Na]^+$. Anal. Calcd for $C_{19}H_{24}N_4O_3$: C, 64.03; H, 6.79; N, 15.72. Found: C, 64.95; H, 6.73; N, 15.68.

***N*^{9}-(9*H*-Fluoren-9-yl)-2-(hydroxyimino)-*N*^{1}-methylnonanediamide (16).** Compound **16** was prepared from the corresponding α-oxime ester using the procedure described for **5** in 70% yield as a yellow oil. ^{1}H NMR (400 MHz, $CDCl_3$): δ 1.42−1.19 (m, 4H), 1.47−1.43 (m, 2H), 1.66−1.60 (m, 2H), 2.22 (t, J = 7.6 Hz, 2H), 2.50 (t, J = 7.2 Hz, 2H), 2.73 (s, 3H), 6.14 (bs, 1H), 7.26−7.22 (m, 2H), 7.35−7.31 (m, 2H), 7.48 (d, J = 7.2 Hz, 2H), 7.62 (d, J = 7.2 Hz, 2H). ^{13}C NMR (50 MHz, $CDCl_3$): δ 23.1, 25.6, 28.5, 28.9, 36.6 (×2), 54.5, 119.9 (×3), 125.0 (×4), 127.7 (×2), 128.6 (×2), 140.5 (×2), 144.3 (×2), 174.7. MS(ESI) m/z: 392.1 $[M - H]^-$. Anal. Calcd for $C_{23}H_{27}N_3O_3$: C, 70.21; H, 6.92; N, 10.68. Found; C, 70.14; H, 6.90; N, 10.65.

***N*^{9}-(4-(Dimethylamino)phenyl)-2-(hydroxyimino)-*N*^{1}-methylnonanediamide (17).** Compound **17** was prepared from the corresponding α-oxime ester using the procedure described for **5** in 87% yield as a yellow oil. ^{1}H NMR (400 MHz, CD_3OD): δ 1.36 (m, 4H), 1.48 (m, 2H), 1.65 (m, 2H), 2.29 (t, J = 7.5 Hz, 2H), 2.53 (t, J = 7.2 Hz, 2H), 2.7 (s, 3H), 2.85 (s, 6H), 6.72 (d, J = 8.8 Hz, 2H), 7.31 (d, J = 8.8 Hz, 2H). ^{13}C NMR (50 MHz; $CDCl_3$): δ 24.2, 26.1, 26.9, 30.0, 30.4, 37.8, 41.4 (×2), 114.5 (×2), 123.0 (×2), 130.0, 149.5, 150.2, 155.1, 166.9, 174.3. MS(ESI) m/z: 370.8 $[M + Na]^+$. Anal. Calcd for $C_{18}H_{28}N_4O_3$: C, 62.05; H, 8.10; N, 16.08. Found: C, 61.98; H, 8.07; N, 16.01.

***N*^{9}-([1,1′-Biphenyl]-4-yl)-2-(hydroxyimino)-*N*^{1}-methylnonanediamide (18).** Compound **18** was prepared from the corresponding α-oxime ester using the procedure described for **5** in 52% yield as a white solid. Mp 177−180 °C. ^{1}HNMR (400 MHz, CD_3OD): δ 1.36 (m, 4H), 1.47 (m, 2H), 1.67 (m, 2H), 2.33 (t, J = 7.6 Hz, 2H), 2.52 (t, J = 7.2 Hz, 2H), 2.76 (s, 3H), 7.25 (t, J = 7.2 Hz, 1H), 7.35 (t, J = 7.2 Hz, 2H), 7.50 (t, J = 7.6 Hz, 4H), 7.57 (d, J = 7.6 Hz, 2H). ^{13}C NMR (100 MHz, $CDCl_3$/CD_3OD) δ: 22.6, 24.8, 25.1 (×2), 28.3, 28.7, 36.4, 119.7, 120.0, 125.9, 126.2, 126.4, 126.5, 126.8 (×2), 128.0, 136.3, 137.4, 140.1, 153.4, 164.9, 172.9. MS(ESI) m/z: 403.8 $[M + Na]^+$. Anal. Calcd for $C_{22}H_{27}N_3O_3$: C, 69.27; H, 7.13; N, 11.02. Found: C, 69.20; H, 7.10; N, 10.99.

***N*^{9}-(3-Bromophenyl)-2-(hydroxyimino)-*N*^{1}-methylnonanediamide (19).** Compound **19** was prepared from the corresponding α-oxime ester using the procedure described for **5** in quantitative yield as a white solid. Mp 142−145 °C. ^{1}H NMR (400 MHz, CD_3OD): δ 1.35 (m, 4H), 1.47 (m, 2H), 1.66−1.64 (m, 2H), 2.32 (t, J = 7.2 Hz, 2H), 2.53 (t, J = 6.8 Hz, 2H), 2.69 (s, 3H), 7.17−7.13 (m, 2H), 7.43−7.41 (m, 1H), 7.85 (bs, 1H). ^{13}C NMR (100 MHz, CD_3OD): δ 22.4, 24.4, 24.8, 25.1, 28.2, 28.6, 36.2, 117.7, 121.4, 122.0, 129.5, 125.9, 139.7, 153.3, 165.1, 172.9. MS(ESI) m/z: 405.7 $[M + Na]^+$. Anal. Calcd for $C_{16}H_{22}BrN_3O_3$: C, 50.01; H, 5.77; Br, 20.79; N, 10.94. Found: C, 49.95; H, 5.74; N, 10.90.

General Procedure of Suzuki Coupling with $Pd[PPh_3]_2Cl_2$ as Catalyst. *N*^{9}-([1,1′-Biphenyl]-3-yl)-2-(hydroxyimino)-*N*^{1}-methylnonanediamide (20). To a solution of **19** (0.026 g, 0.068 mmol) in THF (2 mL), phenylboronic acid (0.025 g, 0.204 mmol), K_2CO_3 (0.056 g, 0.41 mmol), and $Pd(PPh_3)_2Cl_2$ (0.002 g, 0.034 mmol) were added. The suspension obtained was submitted to microwave dielectric heating 2 × 20 min at 110 °C at 200 W. H_2O was used for quenching, and the organic layer was separated. The aqueous phase was extracted several times with ethyl acetate; the organic fractions were collected and dried over anhydrous Na_2SO_4. The solvent was then removed in vacuo. The residue was purified by flash chromatography (petroleum ether/ethyl acetate 4:6) to give the title compound **20** as a white solid (0.015 g, 60%). Mp 128−130 °C. ^{1}H NMR (200 MHz, $CDCl_3$): δ 1.47−1.25 (m, 6H), 1.67 (m, 2H), 2.32 (t, J = 7.6 Hz, 2H), 2.56 (t, J = 7.6 Hz, 2H), 2.76 (d, J = 4.8 Hz, 3H), 5.90 (bs, 1H), 6.82−6.79 (m, 1H), 7.63−7.24 (m, 4H), 7.89−7.69 (m, 2H), 8.26−8.19 (m, 2H), 9.68 (bs, 1H). ^{13}C NMR (50 MHz, CD_3OD): δ 25.0, 26.9, 27.6, 27.7, 30.9, 31.2, 38.8, 120.6, 120.9, 124.5, 128.8 (×2), 129.3, 130.6 (×3), 131.1, 135.6, 141.2, 143.9, 155.9, 175.6. MS(ESI) m/z: 403.8 $[M + Na]^+$. Anal. Calcd for $C_{22}H_{27}N_3O_3$: C, 69.27; H, 7.13; N, 11.02. Found: C, 69.21; H, 7.09; N, 11.00.

3′-(8-(Hydroxyimino)-9-(methylamino)-9-oxononanamido)-[1,1′-biphenyl]-4-carboxylic Acid (21). Compound **21** was prepared from **19** using the procedure described for **20** and obtained in 45% yield as a yellow oil. ^{1}H NMR (400 MHz, CD_3OD): δ 1.55−1.24 (m, 6H), 1.70−1.65 (m, 2H), 2.37 (t, J = 7.2 Hz, 2H), 2.54 (t, J = 7.2 Hz, 2H), 2.79 (s, 3H), 7.38 (d, J = 8.4 Hz, 2H), 7.56−7.53 (m, 2H), 7.98 (d, J = 8.4 Hz, 2H), 8.19 (d, J = 8.4 Hz, 2H). ^{13}C NMR (100 MHz, CD_3OD): δ 22.3, 24.3, 24.9, 25.1, 28.2, 28.6, 36.2, 118.1, 119.0, 122.0, 126.1 (×2), 127.8, 128.6, 129.5 (×2), 132.6, 138.7, 140.2, 144.5, 153.3, 165.1, 173.0. MS(ESI) m/z: 424.1 $[M - H]^-$. Anal. Calcd for $C_{23}H_{27}N_3O_5$: C, 64.93; H, 6.40; N, 9.88. Found: C, 64.99; H, 6.35; N, 9.84.

2-(Hydroxyimino)-*N*^{1}-methyl-*N*^{9}-(3-(pyridine-3-yl)phenyl)nonanediamide (22). Compound **22** was prepared from **19** using the procedure described for **20** in 50% yield (the product is a yellow oil). ^{1}H NMR (400 MHz, CD_3OD): δ 1.52−1.43 (m, 6H), 1.72−1.65 (m, 2H), 2.37 (t, J = 7.6 Hz, 2H), 2.53 (t, J = 7.6 Hz, 2H), 2.75 (s, 3H), 7.36−7.34 (m, 1H), 7.43−7.39 (m, 1H), 7.51−7.48 (m, 1H), 7.57−7.55 (m, 1H), 7.90 (s, 1H), 8.05 (d, J = 8.0 Hz, 1H), 8.50 (s, 1H), 8.76 (s, 1H). ^{13}C NMR (100 MHz, CD_3OD): δ 22.4, 24.3, 24.9, 25.1, 28.2, 28.6, 36.2, 117.9, 119.3, 121.8, 123.7, 128.9, 134.7, 136.5, 137.2, 139.0, 146.5, 147.1, 153.3, 165.0, 173.0. MS(ESI) m/z: 404.8 $[M + Na]^+$. Anal. Calcd for $C_{21}H_{26}N_4O_3$: C, 65.95; H, 6.85; N, 14.65. Found: C, 65.90; H, 6.82; N, 14.68.

***N*^{9}-(3-(6-Chloropyridin-3-yl)phenyl)-2-(hydroxyimino)-*N*^{1}-methylnonanediamide (23).** Compound **23** was prepared from **19** using the procedure described for **24** in 56% yield (the product is a yellow oil). ^{1}H NMR (400 MHz; CD_3OD): δ 1.38 (m, 4H), 1.48 (m, 2H), 1.68 (m, 2H), 2.37 (t, J = 7.2 Hz, 2H), 2.53 (t, J = 7.6 Hz, 2H), 3.28 (s, 3H), 7.35−7.51 (m, 5H), 7.9 (bs, 1H), 8.2 (m, 1H), 8.6 (bs, 1H). ^{13}C NMR (100 MHz; $CDCl_3$): δ 22.4, 24.3, 24.9, 25.1, 28.1, 28.6, 36.2 117.8, 119.4, 121.8, 123.8 (×2), 129.0 (×2), 135.4, 136.3, 137.3, 146.4, 153.3, 165.0 172.9. MS(ESI) m/z: 415.1 $[M - H]^-$. Anal. Calcd for $C_{21}H_{25}ClN_4O_3$: C, 60.50; H, 6.04; Cl, 8.50; N, 13.44. Found C, 60.57; H, 6.01; N, 13.40.

General Procedure of Suzuki Coupling with $Pd_2(dba)_3$ as Catalyst. *N*^{9}-(3-(7-Chloroisoquinolin-4-yl)phenyl)-2-)hydroxyimino)-*N*^{1}-methylnonanediamide (24). A vial containing a magnetic stir bar was charged with $Pd_2(dba)_3$ (0.012 g, 1.0 mol %), P(^{t}Bu)$_3$ (0.01 g, 2 mol %), 7-chloroquinoline-4-boronic acid pinacol (0.075 g, 0.26 mmol), and K_3PO_4 (0.055 g, 0.26 mmol). The vial was sealed with a Teflon-coated cap and then evacuated and backfilled with argon (three times). The aryl halide **19** (0.05 g, 0.13 mmol) and ^{t}BuOH were added sequentially via syringe through the septum. Then the vial was hermetically sealed and the reaction mixture was vigorously stirred at 100 °C for 18 h. The solvent was removed by evaporation in vacuo and the residue was purified by flash chromatography (dichloromethane/methanol 9:1) to yield **24** as a yellow oil (0.028 g, 47%). ^{1}HNMR (400 MHz, $CDCl_3$): δ 1.44−1.31 (m, 4H), 1.49−1.45 (m, 2H), 1.69−1.65 (m, 2H), 2.36 (t, J = 7.2 Hz, 2H), 2.52 (t, J = 7.2 Hz, 2H), 7.21 (d, J = 7.2 Hz, 1H), 2.74 (s, 3H), 7.5−7.45 (m, 3H), 7.52 (d, J= 2 Hz, 1H), 7.55 (d, J= 1.6 Hz, 1H), 7.65 (m, 1H), 7.78 (bs, 1H), 7.94 (d, J= 9.2 Hz, 1H), 8.06 (d, J= 1.6 Hz, 1H), 8.86 (d, J= 4.4 Hz, 1H). ^{13}C NMR (100 MHz; $CDCl_3$): δ 22.4, 24.3, 24.9, 25.1, 28.1, 28.5, 36.1, 119.7, 120.4, 121.1, 124.2, 126.6, 127.1, 127.2, 128.6, 135.1, 137.1, 138.6, 147.8, 148.9, 150.3 (×2), 153.3, 165.1, 173.1. MS(ESI) m/z: 489.2 $[M + Na]^+$. Anal. Calcd for $C_{25}H_{27}ClN_4O_3$: C, 64.30; H, 5.83; Cl, 7.59; N, 12.00. Found: C, 64.34; H, 5.80; N, 11.97.

***tert*-Butyl 6-Oxohexylcarbamate (26).** Compound **26** was prepared following a reported procedure.[22]

Diethyl 2-(6-(*tert*-Butoxycarbonylamino)hexyl)malonate (27). To a solution of the aldehyde **26** (2.05 g, 9.52 mmol) in DMF (10 mL), dimethyl malonate (3.05 g, 2.89 mL, 19.04 mmol) and piperidine (81 mg, 94 μL, 0.952 mmol) were added. The mixture was stirred at room temperature for 1 h. The solvent was removed in vacuo and the mixture was purified by flash chromatography (petroleum ether/ethyl acetate 70:30) to give the expected compound as a colorless oil (2.21 g, 65% yield). This latter was dissolved in MeOH (10 mL), and PtO_2 (28 mg, 0.120 mmol) was added. The mixture was stirred under H_2 at room temperature for 30 min. The catalyst was filtered off and washed with MeOH to give **27** as colorless oil (2.05 g, 92% yield). ^{1}H NMR ($CDCl_3$, 200 MHz): δ 1.12−1.44 (m, 23H), 1.71−1.89 (m, 2H), 2.94−1.05 (m, 2H), 3.21 (t, J = 7.6 Hz, 1H), 4.12 (q, J = 7.2 Hz, 4H). ^{13}C NMR (50 MHz, $CDCl_3$): δ 14.0 (×2), 26.3, 27.1, 28.3 (×3), 28.5, 28.8, 29.8, 51.9 (×2), 61.1 (×2), 78.9, 157.7, 169.4 (×2). MS(ESI) m/z: 382.1 $[M + Na]^+$. Anal. Calcd for $C_{18}H_{33}NO_6$: C, 60.14; H, 9.25; N, 3.90. Found: C, 60.10; H, 9.23; N, 3.88.

Ethyl 8-(*tert*-Butoxycarbonylamino)-2-(hydroxyimino)octanoate (28). Compound **28** was prepared from **27** using the procedure described for **3** in 61% yield (the product is a colorless oil). ^{1}H NMR ($CDCl_3$, 200 MHz): δ 1.25−1.46 (m, 20H), 2.53 (t, J = 7.6 Hz, 2H), 3.02 (t, J = 6.8 Hz, 2H), 4.22 (q, J = 7.2 Hz, 2H). ^{13}C NMR (100 MHz, $CDCl_3$): δ 13.6, 24.1, 25.3, 25.9, 27.9 (×3), 28.7, 29.4, 40.2, 61.1, 78.4, 152.2, 157.1, 163.3. MS(ESI) m/z: 339.1 $[M + Na]^+$. Anal. Calcd for $C_{15}H_{28}N_2O_5$: C, 56.94; H, 8.92; N, 8.85. Found: C, 56.99; H, 8.95; N, 8.83.

8-Amino-2-(hydroxyimino)-*N*-methyloctanamide (29). The α-oxime ester **28** was first converted to the corresponding α-oxime amide using the procedure described for **5** in 75% yield. The product (0.40 g, 1.33 mmol) was then dissolved in CH_2Cl_2 (4 mL), and TFA (1 mL, 13.1 mmol) was added. The mixture was stirred at room temperature for 12 h, the solvent was removed in vacuo, and the mixture was purified by flash chromatography ($CHCl_3$/MeOH 9:1) to give **29** as a yellow oil (0.240 g, 67% yield). ^{1}H NMR ($CDCl_3$, 400 MHz): δ 1.33−1.40 (m, 4H), 1.46−1.50 (m, 2H), 1.59−1.64 (m, 2H), 2.53 (t, J = 7.6 Hz, 2H), 2.76 (s, 3H), 2.89 (t, J = 7.6 Hz, 2H). ^{13}C NMR (100 MHz, $CDCl_3$): δ 22.2, 24.4, 24.9, 25.2, 26.5, 28.2, 38.9, 153.1, 165.1. MS(ESI) m/z: 202.1 $[M + H]^+$. Anal. Calcd for $C_9H_{19}N_3O_2$: C, 53.71; H, 9.52; N, 20.88. Found: C, 53.77; H, 9.55; N, 20.84.

***tert*-Butyl 3-(3-(7-(Hydroxyimino)-8-(methylamino)-8-oxooctylcarbamoyl)isoxazol-5-yl)phenylcarbamate (30).** To a solution of isoxazolecarboxylic acid[15] (0.101 g, 0.33 mmol) in dry THF (3 mL), the amine **29** (0.100 g, 0.49 mmol) was added. The reaction mixture was cooled to 0 °C, and DMTMM (0.164 g, 0.59 mmol) and NMM (0.100 g, 102 μL, 0.99 mmol) were added. The cold bath was removed and the mixture allowed to warm up to room temperature and stirred for 12 h. The white solid was filtered off and the solvent removed in vacuo. The crude mixture was then purified by flash chromatography ($CHCl_3$/MeOH 9:1) to give the title compound **30** as a white solid (0.097 g, 60% yield). Mp 110−112 °C. ^{1}H NMR ($CDCl_3$, 400 MHz): δ 1.37−1.61 (m, 17H), 2.53 (t, J = 7.6 Hz, 2H), 2.75 (s, 3H), 3.27−3.37 (m, 2H), 6.98 (s, 1H), 7.34−7.48 (m, 3H), 7.94 (m, 1H). ^{13}C NMR (100 MHz, $CDCl_3$): δ 24.1, 26.2, 26.9, 27.7, 28.7 (×3), 30.2, 30.3, 40.5, 81.2, 99.9, 116.5, 120.9, 121.7, 128.5, 130.7, 141.6, 155.0, 155.1, 160.6, 161.2, 166.9, 172.7. MS(ESI) m/z: 510.1 $[M + Na]^+$. Anal. Calcd for $C_{24}H_{33}N_5O_6$: C, 59.12; H, 6.82; N, 14.36. Found: C, 59.19; H, 6.80; N, 14.34.

***tert*-Butyl 4-(3-(7-Hydroxyimino-8-(methylamino)-8-oxooctylcarbamoyl)isoxazol-5-yl)phenylcarbamate (31).** Compound **31** was prepared from isoxazole carboxylic acid[15] and **29** using the procedure described for **30** in 65% yield (the product is a white solid). Mp 170−172 °C). ^{1}H NMR ($CDCl_3$, 400 MHz): δ 1.38−1.61 (m, 17H), 2.54 (t, J = 7.2 Hz, 2H), 2.75 (s, 3H), 3.35 (t, J = 7.2 Hz, 2H), 6.98 (m, 1H), 7.54 (d, J = 8.8 Hz, 2H), 7.73 (d, J = 8.8 Hz, 2H). ^{13}C NMR (100 MHz, $CDCl_3$): δ 24.2, 26.2, 26.9, 27.7, 28.6 (×3), 30.2, 30.3, 40.5, 81.3, 98.6, 116.5, 119.6, 122.1, 127.7 (×2), 143.3, 154.8, 155.1, 160.6, 161.4, 166.9, 172.7. MS(ESI) m/z: 510.1 $[M + Na]^+$. Anal. Calcd for $C_{24}H_{33}N_5O_6$: C, 59.12; H, 6.82; N, 14.36. Found: C, 59.07; H, 6.80; N, 14.34.

5-(3-Aminophenyl)-*N*-(7-(hydroxyimino)-8-(methylamino)-8-oxooctyl)isoxazole-3-carboxamide (32). Compound **30** (0.050 g, 0.102 mmol) was dissolved in CH_2Cl_2 (400 μL), and TFA (100 μL, 1.31 mmol) was added. The mixture was stirred at room temperature for 12 h, the solvent was removed in vacuo, and the mixture was purified by flash chromatography ($CHCl_3$/MeOH 9:1) to give **32** as a yellow oil (0.033 g, 85%). ^{1}H NMR ($CDCl_3$, 400 MHz): δ 1.35−1.60 (m, 8H), 2.53 (t, *J* = 7.6 Hz, 2H), 2.75 (s, 3H), 3.28−3.36 (m, 2H), 6.77−6.79 (m, 1H), 6.91 (s, 1H), 7.08−7.20 (m, 3H). ^{13}C NMR (100 MHz, $CDCl_3$): δ 22.3, 24.3, 25.1, 25.8, 28.4, 28.5, 38.7, 97.6, 111.0, 114.3, 116.7, 126.9, 129.1, 148.1, 153.4, 158.7, 159.6, 165.1, 171.6. MS(ESI) *m*/*z*: 410.1 $(M + Na)^+$. Anal. Calcd for $C_{19}H_{25}N_5O_4$: C, 58.90; H, 6.50; N, 18.08. Found: C, 58.93; H, 6.49; N, 18.06.

5-(4-Aminophenyl)-*N*-(7-(hydroxyimino)-8-(methylamino)-8-oxooctyl)isoxazole-3-carboxamide (33). Compound **33** was prepared from **31** using the procedure described for **32** in 81% yield (the product is a yellow solid). Mp 114−116 °C. ^{1}H NMR ($CDCl_3$, 400 MHz): δ 1.36−1.60 (m, 8H), 2.54 (t, *J* = 7.6 Hz, 2H), 2.75 (s, 3H), 3.34 (t, *J* = 7.2 Hz, 2H), 6.73 (s, 1H), 6.74 (t, *J* = 9.6 Hz, 2H), 7.55 (d, *J* = 8.8 Hz, 2H). ^{13}C NMR (100 MHz, $CDCl_3$): δ 22.3, 24.3, 25.1, 25.8, 28.4, 28.5, 38.7, 94.9, 114.1 (×2), 115.4, 126.5 (×2), 149.7, 153.3, 158.6, 159.8, 165.1, 171.9. MS(ESI) *m*/*z*: 410.1 $[M + Na]^+$. Anal. Calcd for $C_{19}H_{25}N_5O_4$: C, 58.90; H, 6.50; N, 18.08. Found: C, 58.96; H, 6.52; N, 18.06.

(3*S*)-3-(Dibenzylamino)-6-vinyltetrahydro-2*H*-pyran-2-one (35). To a solution of aldehyde **34** (1.4 g, 3.5 mmol) in THF (28 mL) vinylmagnesium bromide (1.9 mL, 1.9 mmol, solution 1 M in THF) was added dropwise cooling in an ice−water bath. After the addition, the reaction mixture was allowed to slowly warm to room temperature overnight. The mixture was quenched with saturated aqueous NH_4Cl solution and diluted with ethyl acetate. The organic layer was separated and washed with brine, dried (anhydrous Na_2SO_4), filtered, concentrated, and purified by flash chromatography (petroleum ether/ethyl acetate 9:1) to give a mixture of diastereomeric lactones **35** as colorless oil in 60% yield. ^{1}H NMR (400 MHz, $CDCl_3$): δ 2.04−1.58 (m, 4H$^{\alpha+\beta}$), 3.52−3.38 (m, 1H$^{\alpha+\beta}$), 3.79 (d, *J* = 14 Hz, 2H$^{\alpha+\beta}$), 4.07−3.99 (m, 2H$^{\alpha+\beta}$), 4.69 (m, 1H$^{\alpha+\beta}$), 5.34−5.15 (m, 2H$^{\alpha+\beta}$), 5.83−5.76 (m, 1H$^{\alpha+\beta}$), 7.40−7.23 (m, 10H$^{\alpha+\beta}$). ^{13}C NMR (400 MHz, $CDCl_3$): δ 22.4, 26.3, 27.5, 29.2, 54.9, 55.4, 56.6, 58.1, 81.1, 116.9, 117.2, 127.1, 128.4, 128.5, 128.7, 136.0, 136.1, 139.7, 104.0, 171.1, 172.3. MS(ESI) *m*/*z*: 343.8 $[M + Na]^+$. Anal. Calcd for $C_{21}H_{23}NO_2$: C, 78.47; H, 7.21; N, 4.36. Found: C, 78.40; H, 7.18; N, 4.34.

(6*S*)-6-(Dibenzylamino)-7-oxo-7-(phenylamino)hept-1-en-3-yl Acetate (36). To a solution of aniline (1.32 mL, 16.35 mmol) in CH_2Cl_2 (57 mL), trimethylaluminum (8.2 mL of a 2 M solution in toluene, 16.40 mmol) was added at 0 °C, and the resulting mixture was stirred for 30 min. A solution of **35** (1.75 g, 5.45 mmol) in CH_2Cl_2 (30 mL) was added at 0 °C. After the addition, the reaction mixture was stirred overnight at room temperature. The mixture was quenched with H_2O (3 mL), and an amount of 5 g of anhydrous Na_2SO_4 was added. The resulting mixture was stirred for 30 min, filtered through Celite, washed with ethyl acetate, and concentrated in vacuo. The residue was purified by flash chromatography (petroleum ether/ethyl acetate 7:3) to give a mixture of diastereomeric alcohols in 95% yield. To a solution of this mixture of alcohols (1.72 g, 4.15 mmol) in CH_2Cl_2 (10 mL), triethylamine (2.3 mL, 16.6 mmol), a catalytic amount of DMAP, and acetic anhydride (0.59 mL, 6.2 mmol) were added at 0 °C. The resulting mixture was stirred overnight at room temperature. The reaction was quenched with aqueous NH_4Cl_{ss} and extracted with CH_2Cl_2. The organic extracts were dried (anhydrous Na_2SO_4), filtered, and concentrated in vacuo. Flash chromatography (petroleum ether/ethyl acetate 8:2) gave **36** as a mixture of two diastereoisomers and as a colorless oil (92%). ^{1}H NMR (200 MHz, $CDCl_3$): δ 2.1−1.6 (m, 4H$^{\alpha+\beta}$, 3H, overlapped), 3.31−3.25 (m, 1H), 3.65−3.54 (m, 3H), 3.83 (d, *J* = 13.0 Hz, 2H), 4.15 (m, 1H$^{\alpha+\beta}$), 5.33−5.20 (m, 2H), 5.84 (m, 1H), 7.10 (m, 1H), 7.40−7.24 (m, 12H), 7.53 (m, 2H), 8.90 (d, *J* = 16 Hz, 1H). ^{13}C NMR (400 MHz, $CDCl_3$): δ 14.0, 19.9, 20.4, 20.5, 20.9, 21.1, 21.1, 32.6, 32.6, 54.4, 60.3, 62.3, 62.5, 74.4, 74.6, 116.8, 116.9, 119.0, 119.0, 123.8, 127.4, 127.4, 127.8, 128.0, 128.3, 128.6, 128.9, 136.0, 136.1, 137.6, 137.6, 138.4, 138.5, 170.3, 170.4, 171.1, 171.2, 171.3, 175.6. MS(ESI) *m*/*z*: 478.8 $[M + Na]^+$. Anal. Calcd for $C_{29}H_{32}N_2O_3$: C, 76.29; H, 7.06; N, 6.14. Found: C, 76.36; H, 7.04; N, 6.10.

(*S*)-Diethyl 2-(6((4-Methoxybenzyl)amino)-7-oxo-7-(phenylamino)heptyl)malonate (38). NaH (0.29 g, 7.6 mmol, 60% dispersion in oil) was added to a two-necked round-bottom flask closed with a septum to which dry hexane (2 mL) was added, and the mixture was stirred for 5 min to dissolve the mineral oil. The hexane was removed by a syringe, THF (15 mL) was added, and the resulting mixture was stirred at 0 °C for 10 min. A solution of diethyl malonate (1.7 mL, 11.5 mmol) in THF (15 mL) was then slowly added over 30 min at 0 °C to the resulting suspension. The solution became clear after 10 min of stirring. The stirring was continued for another 30 min. A solution of $PdCl_2(PPh_3)_2$ and PPh_3 in THF (7 mL) was added dropwise at room temperature. After 20 min of stirring, a solution of **36** in THF (15 mL) was slowly added. This mixture was stirred at room temperature overnight. The reaction mixture was concentrated and the residue dissolved in ethyl acetate. A solution of aqueous NH_4Cl was added, and the organic phase was separated and washed with water and brine. The organic extracts were dried (anhydrous Na_2SO_4), filtered, and concentrated in vacuo to give the desired product as a mixture of two regioisomers **37a** and **37b** as colorless oil (80%, ratio **37a**/**37b** is equal to 66:34 from ^{1}H NMR integration analysis of distinct vinyl protons). The product was dissolved in methanol (5 mL) and submitted to H_2 (1 atm) over Pd/C (5%) at room temperature for 2 h. The solvent was evaporated and the residue dissolved in CH_2Cl_2 (6 mL). $NaBH(OAc)_3$ (0.054 g, 0.40 mmol) and acetic acid (few drops) were added, and the mixture was stirred at room temperature for 3 h. The reaction mixture was quenched with H_2O, extracted with CH_2Cl_2, and the organic layer was dried (anhydrous Na_2SO_4), filtered, and concentrated in vacuo. Flash chromatography (petroleum ether/ethyl acetate 9:1) gave **38** as a colorless oil (0.19 g, 46% yield). ^{1}H NMR (200 MHz, $CDCl_3$): δ 1.29−1.19 (m, 10 H), 1.5−1.92 (m, 6H), 3.1−3.4 (m, 2H), 3.68 (d, *J* = 7.2 Hz, 2H), 3.77 (s, 3H), 4.16 (q, *J* = 7.2 Hz, 4H), 6.83 (d, *J* = 7.6 Hz, 2H), 7.11−7.04 (m, 1H), 7.38−7.19 (4H), 7.55 (d, 7.6 Hz, 2H), 9.34 (bs, 1H). MS(ESI) *m*/*z*: 498.8 $[M + H]^+$. Anal. Calcd for $C_{28}H_{38}N_2O_6$: C, 67.45; H, 7.68; N, 5.62. Found: C, 67.40; H, 7.64; N, 5.59. $[\alpha]_D$ −22.5 (*c* 1.0, $CHCl_3$).

(*S*)-Ethyl 8-((*tert*-Butoxycarbonyl)(4-methoxybenzyl)amino)-2-(hydroxyimino)-9-oxo-9-(phenylamino)nonanoate (39). Compound **39** was prepared from the corresponding N-protected derivative using the procedure described for **3** in 50% yield (the product is a colorless oil). ^{1}H NMR (200 MHz, $CDCl_3$): δ 0.85−2.15 (m, 22H), 3.83 (bs, 3H), 4.49−4.22 (m, 5H), 7.45−6.75 (m, 9H). MS(ESI) *m*/*z*: 577.8 $[M + Na]^+$. Anal. Calcd for $C_{30}H_{41}N_3O_7$: C, 64.85; H, 7.44; N, 7.56. Found: C, 64.89; H, 7.41; N, 7.53. $[\alpha]_D$ −63.6 (*c* 1.0, $CHCl_3$).

(*S*)-*tert*-Butyl (8-(Hydroxyimino)-9-(methylamino)-1,9-dioxo-1-(phenylamino)nonan-2-yl)(4-methoxybenzyl)carbamate (40). Compound **40** was prepared from **39** using the procedure described for **5** in 70% yield (the product is colorless oil). ^{1}H NMR (200 MHz, $CDCl_3$): δ 1.42−1.23 (m, 13H), 1.76 (m, 2H), 2.03 (m, 2H), 2.57 (m, 2H), 2.81 (d, *J* = 4.8 Hz, 3H), 3.75 (bs, 3H), 4.37−4.88 (m, 3H), 7.26−6.68 (m, 9H), 8.64 (bs, 1H). MS(ESI) *m*/*z*: 539.2 $[M - H]^-$. Anal. Calcd for $C_{29}H_{40}N_4O_6$: C, 64.42; H, 7.46; N, 10.36. Found: C, 64.36; H, 7.44; N, 10.34.

(*S*)-2-(Hydroxyimino)-8-((4-methoxybenzyl)amino)-*N*^{1}-methyl-*N*^{9}-phenylnonanediamide (41). To a solution of **40** (0.015 xg, 0.03 mmol) in CH_2Cl_2, TFA (1 mL) was added. The reaction mixture was stirred for 1 h at room temperature. The solvent was removed under reduced pressure and the residue purified by flash

chromatography (dichloromethane/methanol 9:1) to yield **41** as a colorless oil (82%). ^{1}H NMR (400 MHz, $CDCl_3$): δ 1.47−1.23 (m, 6H), 1.66 (m, 1H), 1.81 (m, 1H), 2.55 (m, 2H), 2.80 (bs, 2H), 3.33 (m, 1H), 3.75 (bs, 5H), 6.68 (bs, 1H), 6.84 (d, J = 8.0 Hz, 2H), 7.08 (m, 1H), 7.23 (m, 2H), 7.30 (m, 3H), 7.57 (d, J = 7.6 Hz, 2H), 9.50 (bs, 1H). ^{13}C NMR (100 MHz, $CDCl_3$): δ 23.1, 25.3, 25.6, 26.0, 29.0, 33.1, 52.2, 55.3, 62.7, 114.1 (×2), 119.6 (×2), 124.3, 129.0 (×4), 129.7, 137.6, 154.2, 158.9, 160.9, 172.0. MS(ESI) m/z: 439.2 $[M - H]^-$. Anal. Calcd for ($C_{24}H_{32}N_4O_4$: C, 65.43; H, 7.32; N, 12.72. Found: C, 65.49; H, 7.34; N, 12.68. $[\alpha]_D$ −18.0 (c 0.1, $CHCl_3$). The enantiomeric integrity the final product was determined via conversion of **41** to the Mosher amide using commercially available (*S*)-(+)-α-methoxy-α-trifloromethylphenylacetyl chloride and (*R*)-(−)-α-methoxy-α-trifloromethylphenylacetyl chloride under Schotten−Baumann conditions. (*S*)-amide: ^{19}F NMR (215 MHz, $CDCl_3$) δ −69.5. (*R*)-amide: ^{19}F NMR (215 MHz, $CDCl_3$) δ −71.3.

(*S*)-Diethyl 2-(6-(Dibenzylamino)-7-oxo-7-(phenylamino)-heptyl)malonate (42). To a solution of two regioisomers **37a** and **37b** (0.1 g, 0.18 mmol) in MeOH (5 mL) was added PtO_2 (0.05 equiv), and the mixture was stirred under H_2 (1 bar) for 10 min. The catalyst was filtered off, and the filtrate was concentrated in vacuo. Flash chromatography (petroleum ether/ethyl acetate 85:15) gave pure **42** as colorless oil (60%). ^{1}H NMR (200 MHz, $CDCl_3$): δ 1.5−1.2 (m, 10 H), 2.1−1.57 (m, 6H), 3.38−3.16 (m, 2H), 3.6 (d, J = 13.2 Hz, 2H), 3.85 (d, J = 13.2 Hz, 2H), 4.2 (q, J = 7.2 Hz, 4H), 7.1 (m, 1H), 7.48−7.2 (m, 13H), 7.55 (m, 1H), 9.0 (bs, 1H). MS(ESI) m/z: 558.8 $[M + H]^+$. Anal. Calcd for $C_{34}H_{42}N_2O_5$: C, 73.09; H, 7.58; N, 5.01. Found: C, 73.19; H, 7.55; N, 4.98. $[\alpha]_D$ −153.6 (c 1.0, $CHCl_3$).

(*S*)-2-(Dibenzylamino)-8-(hydroxyimino)-*N*^{9}-methyl-*N*^{1}-phenylnonanediamide (43). Compound **43** was prepared from appropriate α-oxime ester using the procedure described for **5** in 84% yield (the product is a colorless oil). ^{1}H NMR (400 MHz, $CDCl_3$): δ 1.42 (m, 2H), 1.65−1.54 (m, 5H), 1.95 (m, 1H), 2.62 (m, 2H), 2.83 (d, J = 5.2 Hz, 3H), 3.23−3.2 (m, 1H), 3.56 (d, J = 13.6 Hz, 2H), 3.79 (d, J = 13.6 Hz, 2H), 6.15 (bs, 1H), 7.07 (m, 1H), 7.35−7.24 (m, 12H), 7.49 (d, J = 8.0 Hz, 2H), 8.2 (bs, 1H), 8.94 (s, 1H). ^{13}C NMR (100 MHz, $CDCl_3$): δ 23.4, 24.5, 25.8, 26.0, 28.3, 29.9, 54.6 (×2), 62.8, 119.2 (×2), 123.9, 127.5 (×2), 128.7 (×4), 128.8 (×4), 129.0 (×2), 137.9, 138.8 (×2), 155.7, 163.9, 172.0. MS(ESI) m/z: 523.3 $[M + Na]^+$. Anal. Calcd for $C_{30}H_{36}N_4O_3$: C, 71.97; H, 7.25; N, 11.19, Found: C, 72.05; H, 7.23; N, 11.16. $[\alpha]_D$ −80.5 (c 0.2, $CHCl_3$).

Molecular Modeling Studies. Molecular modeling calculations were performed on SGI Origin 200 8XR12000 and E4 Server Twin 2 × Dual Xeon 5520, equipped with two nodes. Each node was 2 × Intel Xeon QuadCore E5520, 2.26 GHz, 36 GB RAM. The molecular modeling graphics were carried out on SGI Octane 2 workstations. Experimentally determined structures of human histone deacetylase HDAC 2 (PDB code 3MAX); HDAC 4 (PDB codes 2VQW, 2VQV, 2VQJ, 2VQM, 2VQO, and 2VQQ); HDAC 7 (PDB codes 3C0Y, 3C0Z, and 3C10) and HDAC 8 (PDB codes 3EW8, 3EWF, 3EZP, 3EZT, 3F06, 3F07, 3F0R, 2V5W, 2V5X, 1W22, 1VKG, 1T69, 1T67, and 1T64) were downloaded from the Protein Data Bank (PDB, http://www.rcsb.org/pdb/) and analyzed using the homology module of Insight 2005 (Accelrys, San Diego, CA). Hydrogens were added to all the PDB structures assuming a pH of 7.2. Sequence alignments of all human histone deacetylase were performed using PROMALS3D server (http://prodata.swmed.edu/promals3d/promals3d.php).[23]

Conformational Analysis. The apparent pK_a values of newly designed compounds **2**−**5**, **14**, **17**, **18**, **20**, **22**−**23**, **32**, **33**, **40**, **41**, and **43**, in their tautomeric forms, were estimated using the pharma algorithms of ACD/pKa DB, version 12.00, software (Advanced Chemistry Development Inc., Toronto, Canada). Accordingly, the percentage of neutral/ionized forms was computed at pH 7.2 (cytoplasm) using the Handerson−Hasselbalch equation. Compounds **2**−**5**, **14**, **17**, **18**, **20**, **22**−**23**, **32**, **33**, **40**, **41**, and **43** were built taking into account the prevalent ionic forms of each tautomer at the considered pH value (i.e., 7.2) using the Insight 2005 Builder module. Partial charges were assigned by using the CVFF force field.[24] The conformational space of compounds was sampled through 200 cycles of simulated annealing. An initial temperature of 1000 K was applied to the system for 1000 fs with the aim of surmounting torsional barriers. Successively, temperature was linearly reduced to 300 K with a decrement of 0.5 K/fs. The resulting structures were subjected to an energy minimization protocol within the Insight 2005 Discovery module (CVFF force field, conjugate gradient algorithm; maximum rms derivative of <0.001 kcal/Å; ε = 1). In order to properly analyze the electronic properties, all conformers, obtained from molecular dynamics and mechanics calculations, were subjected to a full geometry optimization through semiempirical calculations, using the quantum mechanical method PM6 in the Mopac2009 package.[25,26] The EF (eigenvector following routine) algorithm of geometry optimization was used, with a GNORM value set to 0.01. To reach a full geometry optimization, the criterion for terminating all optimizations was increased by a factor of 100, using the keyword PRECISE. All resulting PM6 conformers were subsequently ranked by (i) conformational energy (ΔE < 5 kcal), (ii) interatomic distance between the oxime carbon of ZBG and the Cap centroid (distance: <5 Å, 5−7.5 Å, 7.5−10 Å, >10 Å), (iii) torsional angles (amide bonds conformation (cis and trans), oxime configuration (*E* and *Z*)), and (iv) intramolecular hydrogen bonds. Since all inhibitors crystallized into HDAC enzymes show an extended conformation of the linker, in order to analyze both the conformational preferences and the ability to coordinate zinc of newly compounds α-oxime amide ZBG, the most stable stereoisomers of the main tautomer of **5** with an extended conformation (distance ZBG-CAP of >7.5 Å) were selected for DFT calculations. Moreover, X-ray structures of metal oximes complexes (CSD codes BICFUP, CABTUU, CAYCIP, CAYCOV, CAYDEM, EYOTER, FIDWOF, FIDWUL, GIFSAF, GEPMET, IXEBIW, LOVQUI, MEHZUU, WASXEV, ZUDLUF) and metal-amide complexes (CSD codes BUNWEN, LUHBUL) were selected and downloaded from the Cambridge Structural Database (CSD) using the CSDS (Cambridge Structural Database System) software Conquest 1.12. These complexes were analyzed using Insight 2005 (Accelrys, San Diego, CA).

Density Functional Calculations. The selected PM6 conformers of **5**, both in their basic conformation and in complex with Zn^{2+} cation, were optimized at the density functional level of theory by B3 exchange,[27] Lee, Yang, and Parr (LYP) correlation functionals.[28] 6-311++G** basis set functions were used for nonmetal atoms,[29] while LanL2DZ pseudopotential and related basis set were chosen for zinc.[30] The presence of diffuse functions allowed an adequate representation of anionic species molecular orbitals. Any geometrical constraint was imposed during the optimization process. Vibrational frequency calculations at the same level of theory were ensured to verify that every structure represents a minimum on the potential energy surface and zero point correction was included in all energies. The metal complexes binding energies (BE) were determined by considering the coordination of zinc to the ZBG portion of oximes as

$$BE = \sum_{i}^{\text{products}} E_i - \sum_{j}^{\text{reactants}} E_j$$

The BE evaluation was considered in absolute value in order to classify the coordination compounds according to the ZBG-metal bond strength. Zn^{2+} and oximes represent the reactants that give rise to the product as metal complex. As we were interested in the metal−ligands interaction, we performed the natural bond orbital (NBO) analysis of every minimum to elucidate the features of the connection to zinc.[31] The consequences of the metal retrodonation to ligands, according to the electroneutrality principle, were highlighted through the atomic charges evaluations, both in oximes and in zinc complexes. The methodology used to calculate the atomic charges was the atomic polar tensor (APT),[32] which provides values more

reliable than Mulliken and natural population analysis approaches especially for organometallic compounds.[33] All calculations were carried out by the Gaussian 09 suite of programs.[34]

Docking Procedure. In order to find the bioactive conformation, docking studies were carried out on **32** and **41** in complex with human histone deacetylase HDAC 7 (PDB code 3C0Y), using a docking methodology (Affinity, SA_Docking; Insight2005, Accelrys, San Diego, CA) which considers all the systems flexible (i.e., ligand and protein). Atomic potentials were assigned using the esff.frc,[35] a force field including zinc parameters, while the atomic partial charges were assigned using the CVFF force field. Although in the subsequent dynamic docking protocol all the systems were perturbed by means of Monte Carlo and simulated annealing procedures, nevertheless the dynamic docking procedure formally requires a reasonable starting structure. In order to define the ZBG starting conformation of **32** and **41**, all conformers of **5** in complex with Zn^{2+} cation, obtained from DFT calculations, were placed in the active site of experimentally determined structures of human HDACs and superimposed on both the substrate and the inhibitors, taking into account the coordination atoms and the catalytic zinc ion. The conformations that did not show any steric overlap with catalytic-site amino acids were selected as ZBG starting conformations for docking calculations. Accordingly, PM6 conformers of **32** and **41** characterized by a five-membered coordination ring (N−N) or a six-membered coordination ring (O−O) and by a linker extended conformation (distance ZBG-CAP > 7.5 Å) were selected. The ligands were placed in the active site of the enzyme on the basis of previously reported analysis on ZBG and on the basis of the orientation of crystallized inhibitors. On the other hand, for the HDAC enzyme, the crystal structure of catalytic domain of human histone deacetylase HDAC 7 (PDB code 3C0Y) was selected and the water molecules were maintained in the crystal structure with the exception of those that would sterically overlap with the ligands. Flexible docking was achieved using the Affinity module in the Insight 2005 suite, setting the SA_Docking procedure[36] and using the Cell_Multipole method for nonbond interactions.[37] A binding domain area was defined as a flexible subset around the ligand that consisted of all residues and water molecules having at least one atom within a 10 Å radius from any given ligand atom. This binding area was enlarged in order to allow the conformational change at the structural zinc-binding domain. In particular, water molecules and residues having at least one atom within 10 Å radius from structural zinc ion were added to the binding area. All atoms included in the binding domain area were left free to move during the entire course of docking calculations, whereas a tethering restraint was applied on zinc and potassium binding domains, in order to avoid unrealistic results. In particular, the distance between the amino acid coordination atoms and the ions was constrained within 2.5 Å using a force constant of 100 (kcal/mol)/Å. Moreover, in order to obtain more representative results, we increased the variance of docking procedure, applying for each selected starting complex a tether restraint on ligand coordination atoms or on only a single coordination atom. The selected atoms were tethered with a force constant of 30 kcal/Å^2. A Monte Carlo/minimization approach for the random generation of a maximum of 20 acceptable ligand/enzyme complexes, for each compound, was used. During the first step, starting from the previously obtained roughly docked structures, the ligand was moved by a random combination of translation, rotation, and torsional changes (Flexible_Ligand option, considering all rotatable bonds) to sample both the conformational space of the ligand and its orientation with respect to the enzyme (MxRChange = 3 Å; MxAngChange = 180°). During this step, van der Waals (vdW) and Coulombic terms were scaled to a factor of 0.1 to avoid very severe divergences in the Coulombic and vdW energies. If the energy of a complex structure resulting from random moves of the ligand was higher by the energy tolerance parameter than the energy of the last accepted structure, it was not accepted for minimization. To ensure a wide variance of the input structures to be successively minimized, an energy tolerance value of 10^6 kcal/mol from the previous structure has been used. After the energy minimization step (conjugate gradient, 2500 iterations, $\varepsilon = 1$), an energy check criterion (energy range of 50 kcal/mol) and a structure similarity check (rms tolerance of 0.3 kcal/Å) were applied to select the 20 acceptable structures. Each subsequent structure was generated from the last accepted structure. All the accepted complexes resulting from the Monte Carlo/minimization approach were subjected to a molecular dynamics simulated annealing protocol, including 5 ps of a dynamic run divided in 50 stages (100 fs each) during which the temperature of the system was linearly decreased from 500 to 300 K (Verlet velocity integrator; time step of 1.0 fs). In simulated annealing, the temperature is altered in time increments from an initial temperature to a final temperature. The temperature is changed by adjusting the kinetic energy of the structure (by rescaling the velocities of the atoms). Molecular dynamics calculations were performed using a constant temperature and constant volume (*NVT*) statistical ensemble and the direct velocity scaling as temperature control method (Temp Window = 10 K). In the first stage, initial velocities were randomly generated from the Boltzmann distribution, according to the desired temperature, while during the subsequent stages initial velocities were generated from Dynamics Restart Data. A temperature of 500 K was applied with the aim of surmounting torsional barriers, thus allowing an unconstrained rearrangement of the ligand and the heme (initial vdW and Coulombic scale factors of 0.1). Temperature was successively linearly reduced to 300 K in 5 ps, and concurrently the scale factors have been similarly decreased from their initial values (0.1) to their final values (1.0). A final round of 10^4 minimization steps (conjugate gradient, $\varepsilon = 1$) followed the last dynamics steps, and the minimized structures were saved in a trajectory file. After this procedure, the resulting docked complexes were ranked by their conformational energy. In order to choose the structure representing the most probable binding mode, taking into account all experimentally determined structures of human HDACs crystallized in complex with inhibitors, all resulting docked complexes were analyzed and selected by discarding those presenting the inhibitor with a cis alkyl chain or amide bond conformation (Homology module of Insight 2005 (Accelrys, San Diego, CA)). The geometry of $\pi-\pi$ interactions was evaluated considering[38] (i) the distance between the centroids of the aromatic rings, (ii) the angle between the planes of the rings, (iii) the offset value, and (iv) the direction of the dipole vectors.

■ ASSOCIATED CONTENT

Ⓢ Supporting Information. Tables of conditions for Suzuki couplings on the free oxime amide **19**, multiple sequences alignment of classes I and IIa HDAC enzymes interacting regions, analysis of all human HDAC X-rays, X-ray structure of **3**, and comparison between HDAC 7 and HDAC 8 loop Gly763-Pro767 (human HDAC 7 numbering). This material is available free of charge via the Internet at http://pubs.acs.org.

■ AUTHOR INFORMATION

Corresponding Author

*For W.C.: phone, +390691394441; fax, +390691393638; e-mail, Walter.Cabri@sigma-tau.it. For C.F.: phone, +39081678544; fax, +39081678552; e-mail, cfattoru@unina.it. For M.R.: phone, +39089969254; fax, +39089969602; e-mail, mrodriquez@unisa.it.

■ ACKNOWLEDGMENT

We thank Dr. Francesco Berrettini (C.I.A.D.S., University of Siena, Italy) for assistance in X-ray analysis. We thank also Fabio

Vaiano and Davide Paoletti (University of Siena) for skillful technical assistance.

■ ABBREVIATIONS USED

HDACs, histone deacetylases; HDACIs, histone deacetylase inhibitors; SAHA, suberoylanilide hydroxamic acid; ZBG, zinc binding group; CDI, 1,1′-carbonyldiimidazole; APHA, aroylpyrrolylhydroxyamides; CTCL, cutaneous T-cell lymphoma; DMTMM, 4-(4,6-dimethoxy[1,3,5]triazin-2-yl)-4-methylmorpholinium chloride; NMM, 1-methylmorpholine; PMB, *p*-methoxybenzyl; SARs, structure−activity relationships; SA, simulated annealing; MM, molecular mechanics; DFT, density functional theory; CSD, Cambridge Structural Database; PDB, Protein Data Bank; TFMK, trifluoromethylketone; EF, eigenvector following; BE, binding energy; NBO, natural bond orbital; APT, Atomic Polar Tensor; vdW, van der Waals

■ REFERENCES

(1) (a) Bertrand, P. Inside HDAC with HDAC inhibitors. *Eur. J. Med. Chem.* **2010**, *45*, 2095–2116. (b) Paris, M.; Porcelloni, M.; Binaschi, M.; Fattori, M. Histone deacetylase inhibitors: from bench to clinic. *J. Med. Chem.* **2008**, 1505–1529. (c) Rodriquez, M.; Aquino, M.; Bruno, I.; De Martino, G.; Taddei, M.; Gomez-Paloma, L. Chemistry and biology of chromatin remodeling agents: state of art and future perspectives of HDAC inhibitors. *Curr. Med. Chem.* **2006**, *13*, 1119–1139. (d) Miller, T. A.; Witter, D. J.; Belvedere, S. Histone deacetylase inhibitors. *J. Med. Chem.* **2003**, *46*, 5097–5116.

(2) (a) Deal watch: Celgene acquires Gloucester Pharmaceuticals, gaining approved HDAC inhibitor. *Nat. Rev. Drug Discovery* **2010**, *9*, 94. (b) Grant, S.; Easely, C.; Kirkpatrick, P. Vorinostat. *Nat. Drug Discovery Rev.* **2007**, *6*, 21–22.

(3) (a) Cardinale, J. P.; Sriramula, S.; Pariaut, R.; Guggilam, A.; Mariappan, N.; Elks, C. M.; Francis, J. HDAC inhibition attenuates inflammatory, hypertrophic, and hypertensive responses in spontaneously hypertensive rats. *Hypertension* **2010**, *56*, 437–444. (b) Dietz, K. C.; Casaccia, P. HDAC inhibitors and neurodegeneration: at the edge between protection and damage. *Pharmacol. Res.* **2010**, *62*, 11–17. (c) Patil, V.; Guerrant, W.; Chen, P. C.; Gryder, B.; Benicewicz, D. B.; Khan, S- I.; Tekwani, B. L.; Oyelere., A. K. Antimalarial and antileishmanial activities of histone deacetylase inhibitors with triazole-linked cap group. *Bioorg. Med. Chem.* **2010**, *18*, 415–425. (d) Wang, L.; de Zoeten, E. F.; Greene, M. I.; Hancock, W. W. Immunomodulatory effects of deacetylase inhibitors: therapeutic targeting of FOXP3 + regulatory T cells. *Nat. Rev. Drug Discovery* **2009**, *8*, 969–98. (e) Welberg, L. Neurodegenerative disorders: HDAC2 is the one. *Nature Rev. Drug Discovery* **2009**, *8*, 538–539. (f) Kazantsev, A. G.; Thompson, L. M. Therapeutic application of histone deacetylase inhibitors for central nervous system disorders. *Nature Rev. Drug Discovery* **2008**, *7*, 854–868.

(4) Flipo, M; Charton, M.; Hocine, A.; Dassonneville, S.; Deprez, B.; Deprez-Poulain, B. Hydroxamates: relationships between structure and plasma stability. *J. Med. Chem.* **2009**, *52*, 6790–6802.

(5) (a) Jones, P.; Altamura, S.; Chakravarty, P. K.; Cecchetti, O.; De Francesco, R.; Gallinari, P.; Ingenito, R.; Meinke, P. T.; Petrocchi, A.; Rowley, M.; Scarpelli, R.; Serafini, S.; Steinkuehler, C. A series of novel, potent, and selective histone deacetylase inhibitors. *Bioorg. Med. Chem. Lett.* **2006**, *16*, 5948–5952. (b) Suzuki, T.; Miyata, N. Epigenetic control using natural products and synthetic molecules. *Curr. Med. Chem.* **2006**, *13*, 935–958. (c) Dehmel, F.; Ciossek, T.; Maier, T.; Weinbrenner, S.; Schmidt, B.; Zoche, M.; Beckers, T. Trithiocarbonates—exploration of a new head group for HDAC inhibitors. *Bioorg. Med. Chem. Lett.* **2007**, *17*, 4746–4752. (d) Chen, B.; Petukhov, P. A.; Jung, M.; Velena, A.; Eliseeva, E.; Dritschilo, A.; Kozikowski, A. P. Chemistry and biology of mercaptoacetamides as novel histone deacetylase inhibitors. *Bioorg. Med. Chem. Lett.* **2005**, *15*, 1389–1392. (e) Suzuki, T.; Matsuura, A.; Kouketsu, A.; Hisakawa, S.; Nakagawa, H.; Miyata, N. Design and synthesis of non-hydroxamate histone deacetylase inhibitors: identification of a selective histone acetylating agent. *Bioorg. Med. Chem.* **2005**, *13*, 4332–4342. (f) Vasudevan, A.; Ji, Z.; Frey, R. R.; Wada, C. K.; Steinman, D.; Heyman, H. R.; Guo, Y.; Curtin, M. L.; Guo, J.; Li, J.; Pease, L.; Glaser, K. B.; Marcotte, P. A.; Bouska, J. J.; Davidsen, S. K.; Michaelides, M. R. Heterocyclic ketones as inhibitors of histone deacetylase. *Bioorg. Med. Chem. Lett.* **2003**, *13*, 3909–3913. (g) Moradei, O.; Maroun, C. R.; Paquin, I.; Vaisburg, A. Histone deacetylase inhibitors: latest developments, trends and prospects. *Curr. Med. Chem.: Anti-Cancer Agents* **2005**, *5*, 529–560. (h) Hanessian, S.; Vinci, V.; Auzzas, L.; Marzi, M.; Giannini, G. Exploring alternative Zn-binding groups in the design of HDAC inhibitors: squaric acid, *N*-hydroxyurea, and oxazoline analogues of SAHA. *Bioorg. Med. Chem. Lett.* **2006**, *16*, 4784–4787.

(6) (a) Rodriquez, M.; Terracciano, S.; Cini, E.; Settembrini, G.; Bruno, I.; Bifulco, G.; Taddei, M.; Gomez-Paloma, L. Total synthesis, NMR solution structure, and binding model of the potent histone deacetylase inhibitor FR235222. *Angew. Chem., Int. Ed.* **2006**, *45*, 423–427. (b) Gomez-Paloma, L.; Bruno, I.; Cini, E.; Khochbin, S.; Rodriquez, M.; Taddei, M.; Terracciano, S.; Sadoul, K. Design and synthesis of cyclopeptide analogues of the potent histone deacetylase inhibitor FR235222. *ChemMedChem* **2007**, *2*, 1511–151. (c) Petrella, A.; D'Acunto, C. W.; Rodriquez, M.; Festa, M.; Tosco, A.; Bruno, I.; Terracciano, S.; Taddei, M.; Gomez-Paloma, L. Effects of FR235222, a novel HDAC inhibitor, in proliferation and apotosis of human leukemia cell lines: role of annexin A1. *Eur. J. Cancer.* **2008**, *44*, 740–749. (d) Di Micco, S.; Terracciano, S.; Bruno, I.; Rodriquez, M.; Riccio, R.; Taddei, M.; Bifulco, G. Molecular modeling studies toward the structural optimization of new cyclopeptide-based HDAC inhibitors modeled on the natural product FR235222. *Bioorg. Med. Chem.* **2008**, *16*, 8635–8642.

(7) (a) Wong, J. C.; Hong, R.; Schreiber, S. L. Structural biasing elements for in-cell histone deacetylase paralog selectivity. *J. Am. Chem. Soc.* **2003**, *125*, 5586–5587. (b) Haggarty, S. J.; Koeller, K. M.; Wong, J. C.; Butcher, R. A.; Schreiber, S. L. Multidimensional chemical genetic analysis of diversity-oriented synthesis-derived deacetylase inhibitors using cell-based assays. *Chem. Biol.* **2003**, *10*, 383–396.

(8) Mahadevan, S. Role of oximes in nitrogen metabolism in plants. *Annu. Rev. Plant Physiol.* **1973**, *24*, 69–88.

(9) (a) Abele, E.; Lukevics, E. Furan and thiophene oximes: synthesis, reactions, and biological activity. *Chem. Heterocycl. Compd.* **2001**, *37*, 141–169. (b) Abele, E.; Abele, R.; Dzenitis, O.; Lukevics, E. Indole and isatin oximes: synthesis, reactions, and biological activity. *Chem. Heterocycl. Compd.* **2003**, *39*, 3–35.

(10) Abele, E.; Abele, R.; Rubina, K.; Lukevics, E. Quinoline oximes: synthesis, reactions, and biological activity. *Chem. Heterocycl. Compd.* **2005**, *41*, 137–162.

(11) Quiroga, A. G.; Cubo, L.; de Blas, E.; Aller, P.; Navarro-Ranninger, C. *Trans* platinum complexes design: one novel water soluble oxime derivative that contains aliphatic amines in *trans* configuration. *J. Inorg. Biochem.* **2007**, *101*, 104–110.

(12) Saglam, N.; Colak, A.; Serbest, K.; Dulger, S.; Guner, S.; Karabocek, S.; Belduz, A. O. Oxidative cleavage of DNA by homo- and heteronuclear Cu(II)-Mn(II) complexes of an oxime-type ligand. *BioMetals* **2002**, *15*, 357–365.

(13) Moore, R. B.; Chapman, J. D.; Mokrzanowski, A. D.; Arnfield, M. R.; McPhee, M. S.; McEwen, A. J. Non-invasive monitoring of photodynamic therapy with ^{99}technetium HMPAO scintigraphy. *Br. J. Cancer* **1992**, *65*, 491–497.

(14) Shivers, J. C.; Hauser, C. R. Synthesis of certain α-amino acid esters from malonic ester. *J. Am. Chem. Soc.* **1947**, *69*, 1264–1265.

(15) Kozikowski, A. P.; Tapadar, S.; Luchini, D. N.; Kim, K. H.; Billadeau, D. D. Use of the nitrile oxide cycloaddition (NOC) reaction for molecular probe generation: a new class of enzyme selective histone deacetylase inhibitors (HDACIs) showing picomolar activity at HDAC6. *J. Med. Chem.* **2008**, *51*, 4370–4373 and references therein.

(16) (a) Raw, S. A. An improved process for the synthesis of DMTMM-based coupling reagents. *Tetrahedron Lett.* **2009**, *50*,

946–948. (b) Falchi, A.; Giacomelli, G.; Porcheddu, A.; Taddei, M. 4-(4,6-Dimethoxy[1,3,5]triazin-2-yl)-4-methyl-morpholinium chloride (DMTMM): a valuable alternative to PyBOP for solid phase peptide synthesis. *Synlett* **2000**, 275–277. (c) Kunishima, M.; Kawachi, C.; Iwasaki, F.; Terao, K.; Tani, S. Synthesis and characterization of 4-(4,6-dimethoxy-1,3,5-triazin-2-yl)-4-methylmorpholinium chloride. *Tetrahedron Lett.* **1999**, *40*, 5327–5330.

(17) (a) Hanessian, S.; Auzzas, L.; Larsson, A.; Zhang, J.; Giannini, G.; Gallo, G.; Ciacci, A.; Cabri, W. Vorinostat-like molecules as structural, stereochemical, and pharmacological tools. *ACS Med. Chem. Lett.* **2010**, *1*, 70–74. (b) Manku, S.; Allan, M.; Nguyen, N.; Ajamian, A.; Rodriguez, J.; Therrien, E.; Wang, J.; Guo, T.; Rahil, J.; Petschner, A. J.; Nicolescu, A.; Lefebvre, S.; Li, Z.; Fournel, M.; Besterman, J. M.; Déziel, R.; Wahhab, A. Synthesis and evaluation of lysine derived sulfamides as histone deacetylase inhibitors. *Bioorg. Med. Chem. Lett.* **2009**, *19*, 1866–1870. (c) Attenni, B.; Ontoria, J. M.; Cruz, J. C.; Rowley, M.; Schultz-Fademrecht, C.; Steinkühler, C.; Jones, P. Histone deacetylase inhibitors with a primary amide zinc binding group display antitumor activity in xenograft model. *Bioorg. Med. Chem. Lett.* **2009**, *19*, 3081–3084. (d) Kinzel, O.; Llauger-Bufi, L.; Pescatore, G.; Rowley, M.; Schultz-Fademrecht, C.; Monteagudo, E.; Fonsi, M.; Paz, O. G.; Fiore, F.; Steinkühler, C.; Jones, P. J. Histone deacetylase inhibitor with antitumor activity in vivo and optimized pharmacokinetic properties. *J. Med. Chem.* **2009**, *52*, 3453–3456. (e) Jones, P.; Altamura, S.; De Francesco, R.; Gonzalez Paz, O.; Kinzel, O.; Mesiti, G.; Monteagudo, E.; Pescatore, G.; Rowley, M.; Verdirame, M.; Steinkuhler, C. A. A novel series of potent and selective ketone histone deacetylase inhibitors with antitumor activity in vivo. *J. Med. Chem.* **2008**, *51*, 2350.

(18) Rodriquez, M.; Taddei, M. A simple procedure for the transformation of L-glutamic acid into the corresponding γ-aldehyde. *Synthesis* **2005**, 493–496.

(19) Galletti, P.; Quintavalla, A.; Ventrici, C.; Giannini, G.; Cabri, W.; Penco, S.; Gallo, G.; Vincenti, S.; Giacomini, D. Azetidinones as zinc-binding groups to design selective HDAC8 inhibitors. *ChemMedChem* **2009**, *4*, 1991–2001.

(20) Wada, C. K.; Frey, R. R.; Ji, Z.; Curtin, M. L.; Garland, R. B.; Holms, J. H.; Li, J.; Pease, L. J.; Guo, J.; Glaser, K. B.; Marcotte, P. A.; Richardson., P. L.; Murphy, S. S.; Bouska, J. J.; Tapang, P.; Magoc, T. J.; Albert, D. H.; Davidsen, S. K.; Michaelides, M. R. Alpha-keto amides as inhibitors of histone deacetylase. *Bioorg. Med. Chem. Lett.* **2003**, *13*, 3331–3335.

(21) Dowling, D. P.; Gantt, S. L.; Gattis, S. G.; Fierke, C. A.; Christianson, D. W. Structural studies of human histone deacetylase 8 and its site-specific variants complexed with substrate and inhibitors. *Biochemistry* **2008**, *47*, 13554–13563.

(22) Xiao, X.; Antony, S.; Kohlhagen, G.; Pommier, Y.; Cushman, M. Design, synthesis, and biological evaluation of cytotoxic 11-aminoalkenylindenoisoquinoline and 11-diaminoalkenylindenoisoquinoline topoisomerase I inhibitors. *Bioorg. Med. Chem.* **2004**, *12*, 5174–5160.

(23) Pei, J.; Kim, B. H.; Grishin, N. V. PROMALS3D: a tool for multiple sequence and structure alignment. *Nucleic Acids Res.* **2008**, *36*, 2295–2300.

(24) Dauber-Osguthorpe, P.; Roberts, V. A.; Osguthorpe, D. J.; Wolff, J.; Genest, M.; Hagler, A. T. Structure and energetics of ligand binding to proteins: *E. coli* dihydrofolate reductase-trimethoprim, a drug receptor system. *Proteins* **1988**, *4*, 31–47.

(25) Stewart, J. J. P. Optimization of parameters for semiempirical methods V: modification of NDDO approximations and application to 70 elements. *J. Mol. Model.* **2007**, *13*, 1173–1213.

(26) Stewart, J. J. P. *MOPAC2009*; Stewart Computational Chemistry: Colorado Springs, CO, U.S., 2008; HTTP://OpenMOPAC.net.

(27) Becke, A. D. Density-functional thermochemistry. III. The role of exact exchange. *J. Chem. Phys.* **1993**, *98*, 5648–5652.

(28) Lee, C.; Yang, W.; Parr, R. G. Development of the Colle–Salvetti correlation-energy formula into a functional of the electron density. *Phys. Rev. B* **1988**, *37*, 785–789.

(29) Frisch, M. J.; Pople, A.; Binkley, J. S. Self-consistent molecular orbital methods. 25. Supplementary functions for Gaussian basis sets. *J. Chem. Phys.* **1984**, *80*, 3265–3269.

(30) (a) Hay, P. J.; Wadt, W. R. Ab-initio effective core potentials for molecular calculations. Potentials for the transition metal atoms Sc to Hg. *J. Chem. Phys.* **1985**, *82*, 270–283. (b) Wadt, W. R.; Hay, P. J. Ab-initio effective core potentials for molecular calculations. Potentials for main group elements Na to Bi. *J. Chem. Phys.* **1985**, *82*, 284–298. (c) Hay, P. J.; Wadt, W. R. Ab-initio effective core potentials for molecular calculations. Potentials for K to Au including the outermost core orbitals. *J. Chem. Phys.* **1985**, *82*, 299–310.

(31) (a) *NBO*, version 3.1: Glendening, E. D.; Reed, A. E.; Carpenter, J. E.; Weinhold F. (b) Foster, J. P.; Weinhold, F. Natural hybrid orbitals. *J. Am. Chem. Soc.* **1980**, *102*, 7211–7218. (c) Reed, E.; Weinhold, F. Natural bond orbital analysis of near-Hartree–Fock water dimer. *J. Chem. Phys.* **1983**, *78*, 4066–4073. (d) Reed, A. E.; Weinstock, R. B.; Weinhold, F. Natural population analysis. *J. Chem. Phys.* **1985**, *83*, 735–746. (e) Reed, A. E.; Weinhold, F. Natural localized molecular orbitals. *J. Chem. Phys.* **1985**, *83*, 1736–1740.(f) Carpenter, J. E. Extension of Lewis Structure Concepts to Open-Shell and Excited-State Molecular Species. Ph.D. Thesis, University of Wisconsin, Madison, WI, 1987. (g) Carpenter, J. E.; Weinhold, F. Analysis of the geometry of the hydroxymethyl radical by the different hybrids for different spins natural bond orbital procedure. *J. Mol. Struct.: THEOCHEM* **1988**, *46*, 41–62. (h) Reed, A. E.; Curtiss, L. A.; Weinhold, F. Intermolecular interactions from a natural bond orbital, donor–acceptor viewpoint. *Chem. Rev.* **1988**, *88*, 899–926.(i) Weinhold, F.; Carpenter, J. E. In *The Structure of Small Molecules and Ions*; Naaman, R., Vager, Z., Eds.; Plenum: New York, 1988; p 227.

(32) Cioslowski, J. A new population analysis based on atomic polar tensors. *J. Am. Chem. Soc.* **1989**, *11*, 8333–8336.

(33) (a) Irshaidat, T. A unique and novel cyclopropylmethyl cation intermediate: a DFT study. *Tetrahedron Lett.* **2008**, *49*, 5894–5898. (b) Naoki, K. J. Density functional theory study of electroreductive hydrocoupling of α,β-unsaturated carbonyl compounds. *J. Org. Chem.* **2006**, *71*, 9203–9207. (c) Faza, O. N.; Lopez, C. S.; Alvarez, R. A.; de Lera, A. R. Mechanism of the gold(I) catalyzed Rautenstraucht rearrangement: a center-to-helix-to-center chirality transfer. *J. Am. Chem. Soc.* **2006**, *128*, 2434–2437. (d) Lev, D. A.; Grotjahn, D. B.; Amouri, H. Reversal of reactivity in diene-complexed *o*-quinone methide complexes: insights and explanations from ab initio density functional theory calculations. *Organometallics* **2005**, *24*, 4240. (e) Sertchook, R.; Boese, A. D.; Martin, J. M. L. Rozen's epoxidation reagent, $CH_3CN{\cdot}HOF$: a theoretical study of its structure, vibrational spectroscopy, and reaction mechanism. *J. Phys. Chem. A* **2006**, *110*, 8275–8281. (f) Iron, M. A.; Lucassen, A. C. B.; Cohen, H.; van der Boom, M. E.; Martin, J. M. L. A computational foray into the formation and reactivity of metallabenzenes. *J. Am. Chem. Soc.* **2004**, *126*, 11699–11710.

(34) Frisch, M. J.; Trucks, G. W.; Schlegel, H. B.; Scuseria, G. E.; Robb, M. A.; Cheeseman, J. R.; Scalmani, G.; Barone, V.; Mennucci, B.; Petersson, G. A.; Nakatsuji, H.; Caricato, M.; Li, X.; Hratchian, H. P.; Izmaylov, A. F.; Bloino, J.; Zheng, G.; Sonnenberg, J. L.; Hada, M.; Ehara, M.; Toyota, K.; Fukuda, R.; Hasegawa, J.; Ishida, M.; Nakajima, T.; Honda, Y.; Kitao, O.; Nakai, H.; Vreven, T.; Montgomery, J. A., Jr.; Peralta, J. E.; Ogliaro, F.; Bearpark, M.; Heyd, J. J.; Brothers, E.; Kudin, K. N.; Staroverov, V. N.; Kobayashi, R.; Normand, J.; Raghavachari, K.; Rendell, A.; Burant, J. C.; Iyengar, S. S.; Tomasi, J.; Cossi, M.; Rega, N.; Millam, J. M.; Klene, M.; Knox, J. E.; Cross, J. B.; Bakken, V.; Adamo, C.; Jaramillo, J.; Gomperts, R.; Stratmann, R. E.; Yazyev, O.; Austin, A. J.; Cammi, R.; Pomelli, C.; Ochterski, J. W.; Martin, R. L.; Morokuma, K.; Zakrzewski, V. G.; Voth, G. A.; Salvador, P.; Dannenberg, J. J.; Dapprich, S.; Daniels, A. D.; Farkas, Ö.; Foresman, J. B.; Ortiz, J. V.; Cioslowski, J.; Fox, D. J. *Gaussian 09*; Gaussian, Inc.: Wallingford, CT, 2009.

(35) Shi, S; Yan, L; Yang, Y; Fisher-Shaulsky, J; Thacher, T. An extensible and systematic force field, ESFF, for molecular modeling of organic, inorganic, and organometallic systems. *J. Comput. Chem.* **2003**, *24*, 1059–1076.

(36) Senderowitz, H.; Guarnieri, F.; Still, W. C. A smart Monte Carlo technique for free energy simulations of multiconformational molecules. Direct calculations of the conformational populations of organic molecules. *J. Am. Chem. Soc.* **1995**, *117*, 8211–8219.

(37) Ding, H. Q.; Karasawa, N.; Goddard, W. A., III. Atomic level simulations on a million particles: the cell multipole method for Coulomb and London non-bond interactions. *J. Chem. Phys.* **1992**, *97*, 4309–4315.

(38) Kim, K. S.; Tarakeshwar, P.; Lee, J. Y. Molecular clusters of π-systems: theoretical studies of structures, spectra, and origin of interaction energies. *Chem. Rev.* **2000**, *100*, 4145–4185.